INSTITUTO SUPERIOR TÉCNICO
Universidade Técnica de Lisboa

Morphing Aircraft Structures

Design and Testing an Experimental UAV

Pedro Manuel Magalhães da Costa Aleixo

Dissertação para obtenção do Grau de Mestre em

Engenharia Aeroespacial

Júri

Presidente: Prof. Afzal Suleman

Orientador: Prof. Fernando Lau

Co-orientador: Prof. Afzal Suleman

Vogal: Prof. Alexandra Gomes

Outubro de 2007

Abstract

This thesis presents the design, build and test of a morphing structure, with the objective of reducing the wing's drag. The results of a computational assessment of the morphing concept benefits are shown. Drag reductions from 5% to nearly 40% at different flight speeds serve as motivation for designing, building and testing a prototype of the wing, [24].

Design requirements of the morphing mechanism structure are pointed out and manufacturing solutions are discussed. The main objective of this work is to prove the feasibility and functionality of the morphing mechanism solutions. The whole fabrication process of the wing is described. The difficulties found during the manufacturing process are presented. Consequently the solutions to mitigate those difficulties are discussed and the one thought to be the best is pointed.

The final wing is shown and described. The adaptations made in consequence of the difficulties found during the manufacturing are explained. As a result, not all the requirements are fulfilled, but the requirements dropped were thought not to have a crucial influence in the aerodynamic performance.

The use of a flexible skin for the morphing wing is described. Skin stretch and rigidity influence on the wing's aerodynamics is studied qualitatively. Three different types of skins, were tested and compared; the best solution was used to perform the tests to prove the concept.

Wind tunnel test results are shown and are submitted to analysis. Different wing planform tests performed with the morphing wing are described and drag reduction is quantified for different airspeeds. The results achieved a drag reduction up to 25% when compared to a fixed wing.

Finally it was found that the wing achieved its purpose and opened a new window to keep the development of these types of wings. Possible further work suggestions are made, such as wing structure and skin developments.

Key-words: morphing wing, structure, drag reduction, prototype, wind tunnel.

Resumo

O trabalho apresentado nesta tese versa sobre o *design*, construção e teste de uma estrutura capaz de alterar a sua forma, com o objectivo de minimizar a resistência ao avanço. Os resultados dos estudos computacionais são apresentados, assim comoas suas vantagens. A redução da resistência de 5% até quase 40%, em diferentes velocidades de voos, servem de motivação para o *design*, construção e teste de um protótipo da asa, [24].

Os requisitos de *design* do mecanismo da estrutura são nomeados e as soluções para a construção são discutidos. O principal objectivo deste trabalho é provar a viabilidade e funcionalidade do mecanismo adaptativo proposto. Todo o processo de fabrico da asa é descrito. As dificuldades encontradas durante o processo são apresentadas, consequentemente as soluções para resolver estes problemas são discutidas e a solução que apresentou melhores condições é implementada.

O modelo final da asa é apresentado e descrito. As adaptações feitas ao modelo, em consequência das dificuldades de construção, são explicadas. Como tal, nem todos os requisitos são cumpridos. No entanto, o requisitos deixados para trás são os que menos influenciam o desmpenho aerodinâmico.

A utilização de um casca flexível é descrita. A influência do nível de extensão e da rigidez da casca na aerodinâmica é qualitativamente estudada. Para tal são usadas três diferentes cascas. Estas cascas foram testadas e a melhor solução foi usada para realizar os testes para provar este conceito.

Os resultados do túnel de vento são mostrados e sujeitos a análise. As diferentes formas da asa adaptativa foram testados para vérias velocidades, sendo a redução da resistência em relação à asa fixa, calculada para cada caso; valores máximos de 25% de redução foram observados.

Finalmente foi concluido que a asa proposta atingiu os seus objectivos e abriu novas janelas para continuar o desenvolvimento desta solução. São feitas sugestões para melhorar a asa proposta, como alterações à estrutura e casca.

Palavras-chave: morphing wing, estrutura, redução de resistência, protótipo, tunel aerodinâmico.

Acknowledgments

This thesis means the end of my graduation, therefore I must be grateful to a lot of persons who helped me and supported me throughout my long journey at Instituto Superior Técnico.

Professor Afzal Suleman gave me the opportunity to work in such a revolutionary and ambitious project I address my acknowledgments.

To José Vale, with whom I had the pleasure to work with, my gratitude for the help and the guidelines that he gave me during the project. Without his help I could never developed my work.

I am thankful to Professor Fernando Lau for his endless efforts to make this thesis better and for the work he is developing to make the course of Aerospace Engineering better, demander and with higher quality.

A special thanks to my colleague mates who made my studies much more interesting for the discussions, different points of views in several subjects and the helpful notes to study. I consider this one of most important part for my work.

I am deeply grateful to Filipa, for her enormous patience to help me in every single issue I needed and her endless support and encouragement during all these times. She has been my pillar.

Finally and the most important, to my family: my mother, Maria, and my sisters, Andrea and Ana, to whom I hardly can express my gratitude and of whom I am very proud. They listened, advised and supported me in all my decisions, which became to me the fountain of strength and courage.

To Maria, Andrea, Ana and Filipa, who have been my foundation and I hope that I made them proud, I dedicate this thesis.

Contents

List of figures

List of Tables

Chapter 1

1 - Introduction

1.1 - Background and Motivation

Airplanes fly under a wide range of temperature, density and wind conditions. They also have to perform different flight manoeuvres during a flight: take off, landing, cruise, climb, coordinated turns and others manoeuvres. To perform efficiently in these conditions the aircraft is required to have different configurations.

The aircrafts are designed to have the best performance in the most important flight stage, which depend on the mission that the aircraft have to accomplish. For commercial aircrafts the most important stage is cruise while for militaries aircrafts usually is manoeuvring. When they fly out of the optimal flight condition, the performance is severely affected. The ability to change the aerodynamic shape to increase the optimal flight envelope is highly desirable. This is a very ambitious goal that motivates aircraft designers to invent and create new innovative solutions for structural concepts.

Aeronautical history is full of innovative solutions to adapt aircraft. For instance, Wright brothers used warping wings to provide lateral control for the *Wright B flyer* by twisting the wings, but this concept vanished from the designers' mind because it requires high energy actuation. At that time there wasn't enough technology to keep developing this solution.

Although fixed wings must operate under the design condition, this is not possible often, especially in aircrafts which have a wide operating range, like surveillance and military aircrafts. For commercial aircrafts during take off, landing and other short flight stages, high-lift devices are used to improve the performance (figure 1).

Figure 1 - *High-lift devices*

Different forms of aerodynamic shape control can be achieved by retractable landing gears, flaps and other devices that are deployed when needed. These devices provide shape control over wing sweep, camber line and wing twist. The majority of aircrafts use these kinds of devices for specific flight stages, *e.g.* flaps are deployed for take off and landing to increase lift at low speeds, by increasing the wing surface and changing its camber line; ailerons change wing twist angle to provide roll control and are used for all types of turns.

Nowadays, researches are being conducted to create airplanes' structures that may radically change their shape in-flight, in order to get the best aircraft shape for the given flight condition. The aircrafts will be able to operate in optimal conditions throughout the entire flight envelope, which will increase their fuel efficiency and manoeuvring capabilities. These aircrafts are called "morphing aircrafts".

The most known morphing technology application is *F-14 TomCat* (figure 2) that changes its sweep angle to strike a balance between range and speed by delaying the rise in drag for higher speeds.

Figure 2 - *F-14 Tom Cat: Unswept and swept wings*

So far, new concepts never have gone further then the experimental state due to the high complexity of structures, the lack of energy efficiency as well as the weight efficiency of the actuation devices. Recently, new technologies and the creation of advanced materials made possible the design of morphing wings that can adapt to a specific flight condition in order to improve the aircraft performance.

The aircraft's performance can be improved by adjusting the span, chord and sweep angle among others. It is important to choose the right parameters to adjust because some may cause undesirable side effects on the performance, others don't change significantly the performance. It is required to know which parameters affect mostly the performance; these parameters are airfoil shape and wing planform. Altering the wing planform changes numerous parameters like span, chord, sweep, dihedral and twist angles; while altering the airfoils shape, changes the thickness and camber line.

Just like birds that adopt different positions to get the best shape for the flight and thus saving their energy, we are looking for an aircraft that adopts the best shape for the given flight conditions and spends the minimum energy possible: aircraft design is inspired by nature.

Introducing morphing capabilities on aircrafts will allow them to fly with minimum drag, having better performance in all flight stages. This has an effect on fuel consumption, range or maximum speed. Other possibility is having aircrafts with the same weight but that are able to carry more payload.

Morphing structures are complex and require several actuation devices, which increase aircraft weight. Manufacturing is thus harder than in fixed wings. As a result, it's necessary to balance the improvement of performance with the increase of complexity and weight.

1.2 - State of the Art

Morphing aircrafts can bring many advantages to aeronautical industries and to militaries. Therefore, a lot of research in this area has been done due to the prospect of large benefits.

The latest research has been made on Unmanned Aerials Vehicles (UAV) with morphing technology and drones, because it is easy to build for experiments due to its size, therefore accessible to universities and students.

The advance in new materials improves the design and new materials are developed everyday. As a result they allow the development of new structures and actuation mechanisms, since they are lighter, reliable and stiffer.

University of Florida has made a research on wings that are able to deform continuously. These wings are very complex and are used on micro aircrafts (figure 3). Flexible wings allow complex wing shapes and are more stable than the rigid ones, especially in unstable weather conditions. Other flexible wings have been developed but unsuccessfully. Flexible wings need to be changed constantly when turbulence is high. Controlling manually the shape of the wing is an impossible task, so new software and hardware are needed to control these wings, [2].

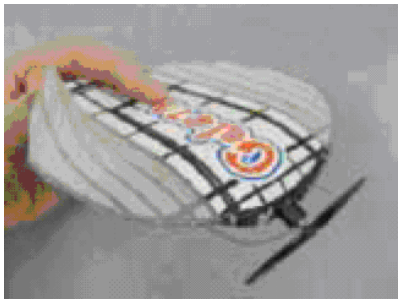

Figure 3 - *Flexible wing on a micro aircraft*

Another research was on segmented wings that change their longitudinal shape (figure 4). The change of the shape is smooth, yet it contains some discontinuities. Experiments proved that controllability may be affected for large movements, although increasing the number of segments increases the stability. A wide range of lift and drag coefficients can be achieved with this morphing technology. Recently, it has been suggested to use micro-deformation using smart materials, avoiding the discontinuities on the wing due to the segments, [1].

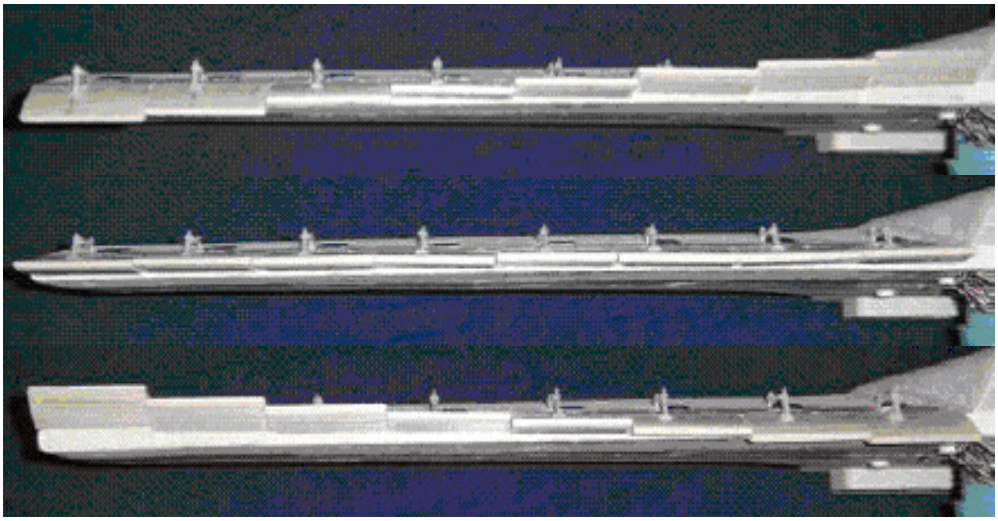

Figure 4 - *Segmented wing*

Hyper elliptic cambered span (HECS) wings are being developed since 2003 by NASA. University of Virginia has designed a HECS wing based on several segments. This wing can increase its planform area in 10% to 15% and reduce drag by augmenting the Oswald coefficient. It is made by several segments that fold, creating an approximated elliptic cambered span. This mechanism uses only one actuator at the wing root. The motion is transmitted by binary links, [22].

Cornell University developed also a HECS wing (figure 5) very similar to Virginia University's one, but it is actuated by smart material alloy wires. This option reveals to be more energy efficient, [12].

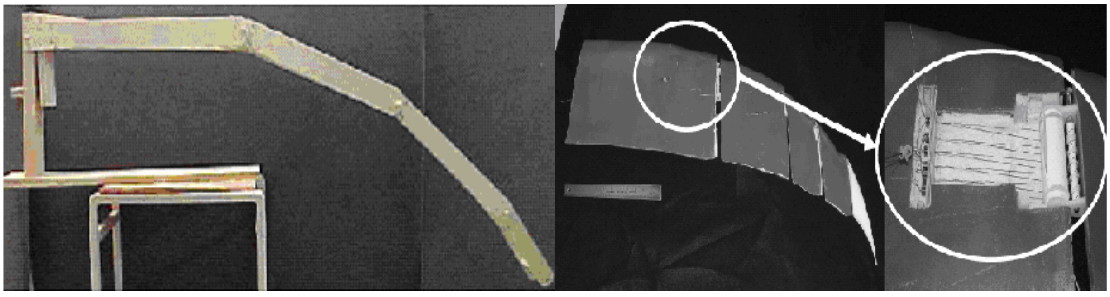

Figure 5 - *HECS wing, on the left: Virginia University; on the right: Cornell University*

An inflatable wing is as well being researched by the University of Kentucky. This wing inflates at high altitude flight and rigidize by the action of UV radiation during the climb, which is done with the help of a balloon, [23]. Researchers from Dover have a similar research (figure 6), but the wing has a conformal flap in the trailing edge, actuated by piezoelectric, that doesn't get rigid. This wing is inflated and deflated

depending on the needs to control rolling movements and is able to change airfoil shapes such as NACA 8318 and NACA 0018, [7].

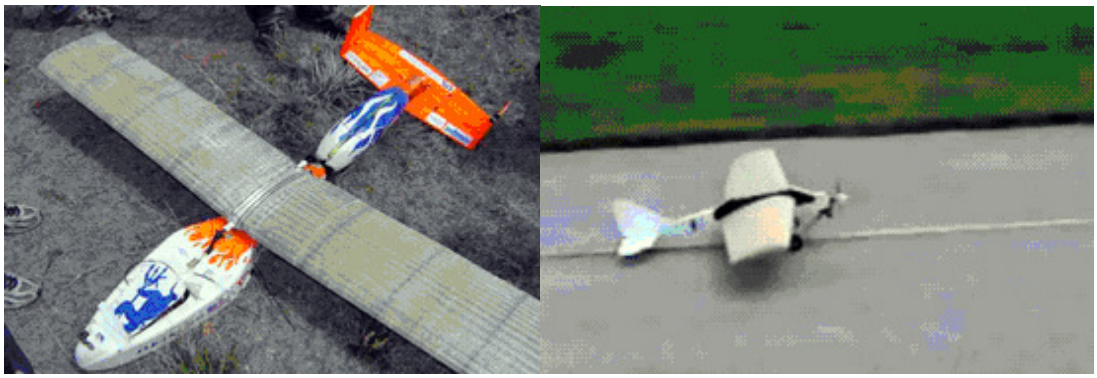

Figure 6 - *Inflatable wings, on the left: University of Kentucky; on the right: Dover*

U.S. Air Force made researches on conformal flaps. These flaps are smoothly varying surfaces and revealed to be more efficient then hinged flaps, since they avoid singularities on the fluid flow mathematical model: the pressure distribution is smoother, providing a higher control performance (figure 7), [18].

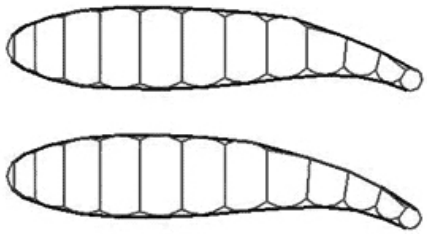

Figure 7 - *Conformal Flaps*

In United Kingdom variable cant winglets are being developed. These winglets are able to change its cant angles (figure 8). They don't replace conventional control surfaces, but the results show that their use improve the fight substantially. The next step of this research is to test a model with multi-axial winglets to replace all conventional control surfaces, [5].

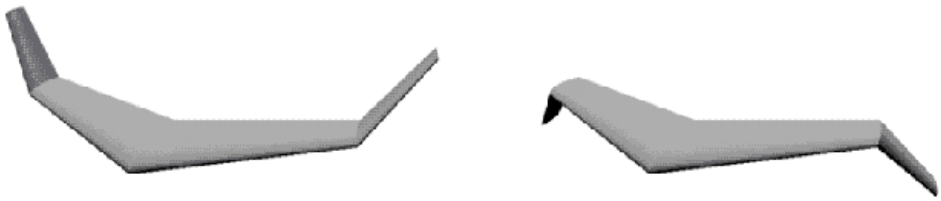

Figure 8 - *Variable cant angles*

New software and powerful computers are being applied on morphing aircrafts, which allows integrating all analysis, leading to a better design and efficiency. Such projects are being conducted at companies like NextGen Aeronautic Inc. and Lockheed Martin. These projects are the latest advances in morphing aircrafts. There are four main configurations that morphing aircrafts should be able to perform in order to keep the optimized shape for the best performance possible: loiter, dash, manoeuvre and cruise (figure 9).

Figure 9 - *Standard, loiter, dash and manoeuvre*

Standard configuration is the best configuration for cruising; this depends on the cruise altitude and cruise speed. Loiter configuration is used for flight stages like surveillance thus low speeds; in general the wing must have high aspect ratio, *i.e.*, large span and small chord. Dash configuration is indicated for high speeds; the span is small, the wing is swept and is tapered. Manoeuvre configuration is appropriated for manoeuvres; small span and large chord and slightly swept.

The aim of these companies is to build a UAV for multiple flight conditions. Numerous wing parameters such as aspect ratio, wing span, sweep angle and chord change during the flight, allowing the wing to change its shape.

The adaptive platform vehicle experiment (APVE) is an UAV design at University of Virginia [19]. This UAV has a telescopic morphing structure in the wings, tail and fuselage. This project was done to assess the benefits obtained in the NextGen Aeronautics Inc. project, since the results are not available (figure 10).

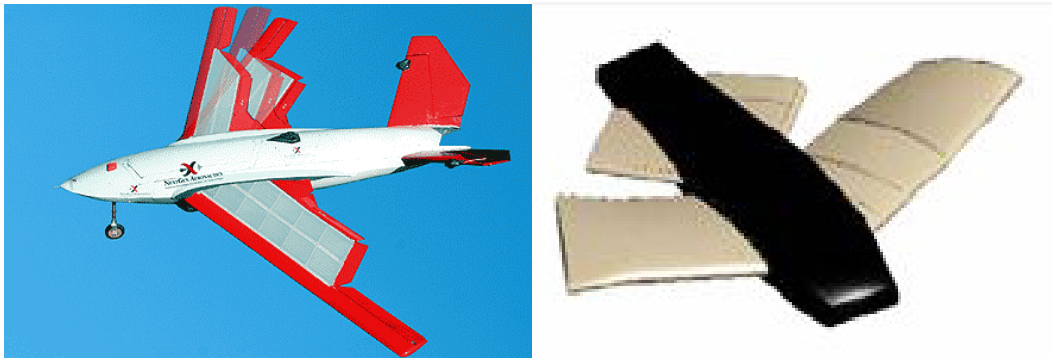

Figure 10 - *Morphing aircrafts, on the left: N-MAS; on the right: APVE*

Lockheed Martin is developing a folding wing: the fully extended configuration is for loitering and the folded configuration for dashing. The wing is able to fold 130º into the fuselage (figure 11), [14].

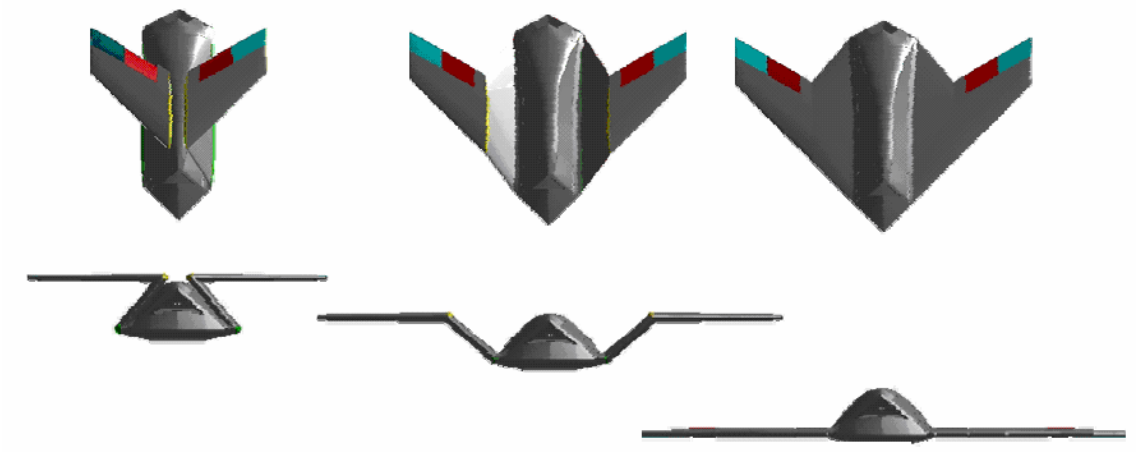

Figure 11 - *Lockheed Martin's morphing aircraft*

Variable-span morphing wings were studied in Virginia Polytechnic Institute and it has been found that this morphing not only improves the aircraft's performance at different flight conditions, but also improves the roll control, when compared to conventional roll controls. This research was conducted to apply these wings to a cruise missile. Even so they found that, when the wing is fully extended instability problems such as flutter are likely to happen sooner (figure 12), [4].

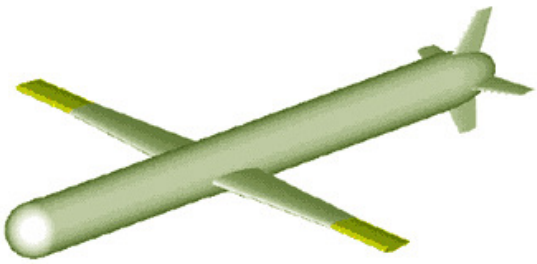

Figure 12 - *Variable Span Morphing Wing*

Materials are very important in aeronautic industry due to the dichotomy of weight and strain, hardness and flexibility and much work has been done to develop a material that can be lighter but stiffer, hard but flexible. In the last years, researches have been focused on composite materials, since it allows both rigid and flexible materials. Projects such as NextGen use flexible composite materials.

Memory shape materials are being researched also. These materials are very promising due to the possibility of changing its shape by the use of an electric sign or by varying the temperature. Bending materials technology is preferable to the segmented wing, since it provides a smooth airfoil, avoiding steps that cause turbulence in the flow. However, smart materials have a long way to go to became reliable, [9].

University of Bristol is researching composite plates that are bi-stable and allow swapping positions. These materials use the orthotropic proprieties to change its position, [11].

Other materials based on nanotechnology and on spider silk are being researched. Nanotechnology [15] is very promising due to its materials properties, since it has a great tensile strength. But there is long way to go on the development of this technology. Spider silk is hard to synthesise and DNA manipulation is on the very first steps, [21].

The University of Virginia found a plastic material that could become the best material for morphing wings (Tecoflex ©), because it requires less force to deform than other tested materials. The other materials that they have tested are shape memory polymers, polyurethanes among others [10].

1.3 - Scope

The present thesis is a part of a wider project that involves aerodynamic and structural optimization. This part of the wider project is to design, build and test a prototype of a morphing wing.

In this thesis I present the design and construction of a morphing wing that changes its chord and span, unlike the ones I have stated before that only changes one parameter: chord, span, dihedral angle or sweep angle. The project of APVE, NextGen and Lockheed also change more than one parameter. Although NextGen and Lockheed projects are not known deeply, due to the fact that they are being developed by companies.

The first part of this thesis was the design of structure that was able to change the chord and the span. Initially the aim was to change the airfoil thickness but this requirement was dropped due to the high complexity that it involves.

The chord has to increase its minimum size of 0.22m to 0.33m, the span of 2.4m to 3.4m, the thickness also varies between 14mm and 25.2mm but that was not possible to accomplish with the means we had.

The design was made using SolidWorks© software after dimensioning the structure based on the loads calculated before. The dimensioning was done by the use of ANSYS© software for numerical calculus; analytically formulas were used for the simple calculus.

Afterwards, we built the prototype. This task took place at IST mechanical facilities. We used the milling machine, the folding machine and the driller, in order to build every parts of the wing's structure: ribs, spars and central blocks.

With the prototype built we made some wind tunnel tests at AFA (Academia da Força Aérea) aeronautical laboratory facility, using their wind tunnel. The wind tunnel tests had the objective of evaluating the wing's performance. Those results were compared with the computational results.

This thesis validates the previous work done and led to a paper published at RTO (Research and Technology Organisation) of NATO last April, [8].

1.4 - Layout

In the second chapter it is summarized the previous studies of aerodynamic shape optimization, structural design and coupled aero-structural analysis. The objective of this morphing wing is to be able to fly with a constant lift, equal to aircraft weight, with the lowest drag possible, [24].

In the third chapter it is presented the wing structural design as well as the options taken and its justifications. In the first part of this chapter we describe the geometric and loads requirements for the wind tunnel and the adaptations made to the wing. Then a description of the wing mechanism concept, its design and all the components are described. Afterwards, the sizing of the mechanism components is done. The manufacturing itself is explained, including the adaptations made during the construction. Finally different skins materials are described.

The fourth chapter describes the method used for the wind tunnel tests, the structure assembled to support the wing in the tunnel. Also we describe the configurations used as well as the objective for each configuration.

Chapter five presents the results and its analysis. First of all, the different skins results are analysed. The best skin is chosen and the results of the different configurations using the chosen skin are presented. The emphasis is on the L vs. D charts, because these are the parameters that show us if morphing wings have advantages over classic wings.

Sixth chapter sets the conclusions and further work to improve this specific morphing wing, by altering the chord and the span.

Chapter 2

2 - Specific Background

In this chapter it is summarized the previous studies of aerodynamic shape optimization, structural design and coupled aero-structural analysis. The objective of this morphing wing is to be able to fly with a constant lift, equal to aircraft weight, with the lowest drag possible, [8, 24].

2.1 - Aerodynamic Shape Optimization

The aerodynamic analysis is done in two steps. First, the 2-dimensional (2D) aerodynamic coefficients as functions of angle of attack and Reynolds number (*Re*) at specified wing sections across the span are obtained. The airfoils are represented by b-spline control points. Then, a non-linear lifting-line method [3] algorithm is used to obtain the lift distribution and induced drag. The lift and the parasite drag are obtained by integrating the lift and parasite drag coefficients corresponding to all local angles of attack. The wing is represented by the chord and incidence at specified sections along the semi-span. The sections' aerodynamic information comes from the previous step. The aerodynamic shape optimization is carried out with the sequential quadratic programming (SQP).

A total of 13 design variables are adopted in this design problem. The design variables are the angle of attack, α, the span of the wing, b, and the chord length, c, at two semi-span positions (the chord where the wing joins the central wing and the tip chord) and the airfoil shape. In this case, the span is allowed to vary between 2.4m and 3.4m and the chord length is limited to a minimum of 0.22m and a maximum of 0.33m. The variation of the chord length between these two design chords is linear. The airfoils at the reference stations can change its thickness and camber distributions only limited by a thickness in the range 14mm to 25.2mm. There is no twist of the wing since the morphing concept does not permit such mechanism and the sweep angle at quarter chord position is kept constant and equal to zero. These geometric constraints are

imposed due to the physical limitations of the morphing mechanisms and the rubber-like material to be used for the skin. A fixed leading edge diameter, ϕ_{LE}, is imposed since the morphing mechanism concept does not allow it to be changed.

The aim of the optimization is to minimize the drag of the wing at speeds between 15m/s and 50m/s. The lift required is the UAV weight of 100N.

The last design variables are the abcissas of the airfoil's b-spline control points coordinates non-dimensionalized by the chord length.

The airfoil resulting from the optimization process is shown in the next figures.

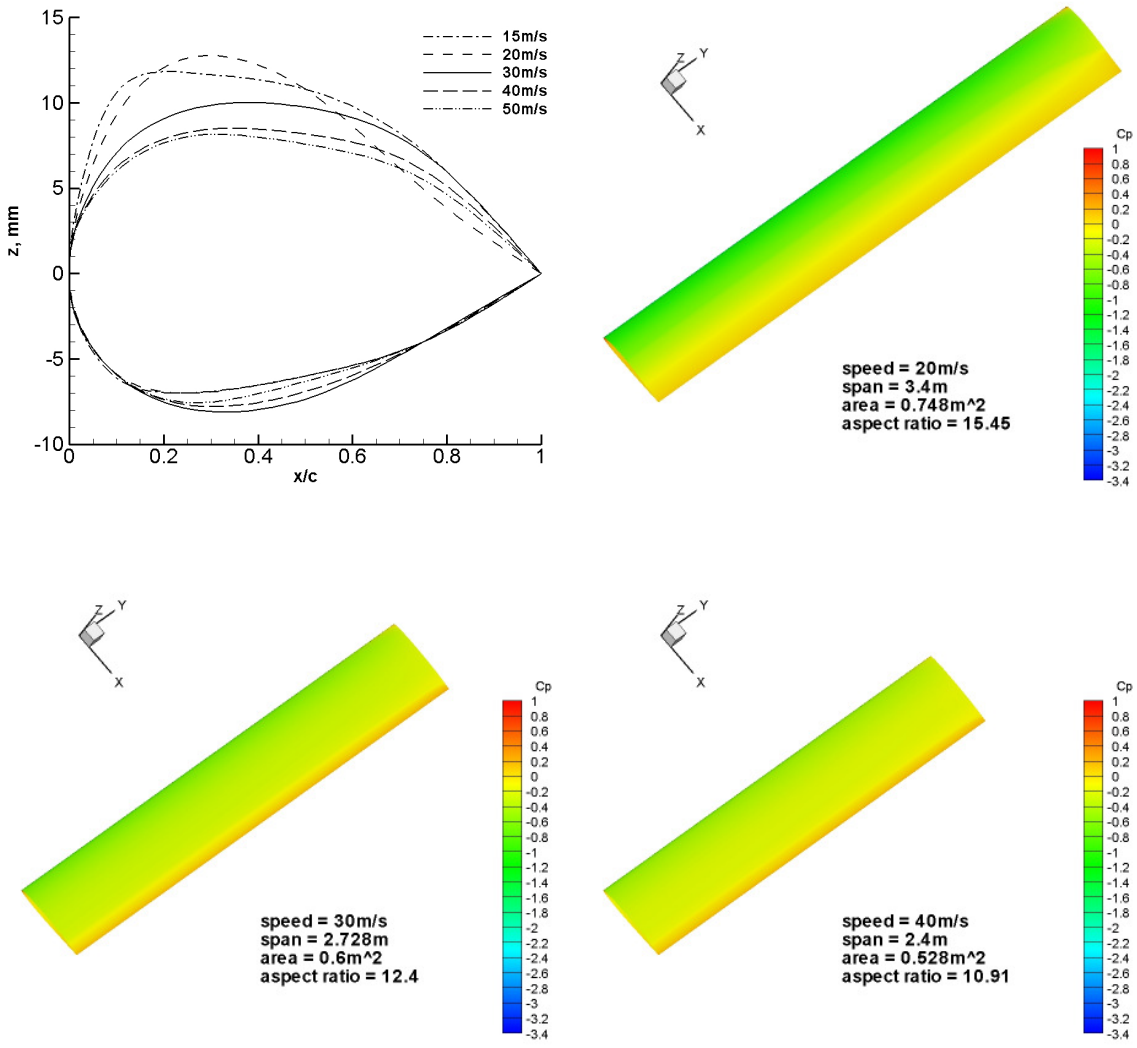

Figure 13 - *Airfoil sections and wing planforms for five speeds*

2.1.1 - Aerodynamic Shape Optimization Results

The optimized geometry of the morphing wing is summarized in figure 13. It can be observed that, as speed reduces, the airfoil thickens up and the camber increases with its maximum value moving slightly forward on the chord. The solution at lower speeds was very much restricted by the airfoil geometry constraints. Since the morphing concept has limited capability to increase thickness, the maximum allowable wing planform area was never attained because, for the maximum chord length, the airfoil becomes so thin (about 6.3% of relative thickness) that its maximum lift coefficient is very low and the extra area is not sufficient to outperform the higher maximum lift coefficient obtained from a slightly thicker airfoil with smaller chord length. The drag results are presented in sub-section 2.4 below together with the drag results of the conventional wing and the deformed wing obtained from the aero-structural analysis.

2.2 - Structural Design

In order to achieve the desired shape changes for the morphing wing, the skin material has to endure high strains, which is not the case with the materials usually used in conventional aircraft. Therefore, rigid materials, as metals or high stiffness/low strain polymer membranes, were ruled out. Rubber materials and other polymers could be considered candidates, including new smart materials as shape memory polymers. Nevertheless, vulcanized rubber was chosen to be the skin material, due to its availability, low price and the desire to prove the feasibility of the morphing concept without much concern about cyclic fatigue or environmental hazard. The use of a shape memory polymer was initially considered, but the increase in complexity of the morphing system due to the heating requirements and the elastic-perfectly plastic behaviour of such material makes its shape memory properties at least unusable when the wing is loaded.

The structural model must not only be capable of increasing the chord at a wing section but also of discretizing the airfoil and allowing changes in airfoil thickness at some control points. In this work, it is considered that the mechanism divides the airfoil in 6 different sections along the chord, three of them being evenly spaced from the quarter chord to the leading edge and the last three sections being evenly spaced from the quarter chord to the trailing edge. The span expansion mechanism is intended to stretch

the wing skin and also maintain the rib expansion mechanisms evenly distributed along the span of the wing.

2.2.1 - Wing FEM Structural Model

The finite element method (FEM) structural model of the wing was built not only to perform the coupled aerodynamic-structural analysis but also to assess the wing deformation forces involved in such a structure. Therefore, the model is required to allow the application of aerodynamic loads on the wing deformable skin and stringers and simulate some of the moving parts of the morphing mechanism in such a way that relevant forces and moments acting on it can be obtained.

Rubber like materials can be modelled in a number of ways when a FEM is applied, traditionally, using a strain energy function dependant only on deviatory deformations. A variety of strain energy functions are supported by Ansys®, the commercial structural analysis program.

For simplicity, the parts of the extension mechanisms of the ribs that are not modelled and the spar extension mechanism are assumed to be rigid enough to support all deformation loads with negligible deformation of their own. In order to avoid the use of surface to surface contact elements, some beam components used for skin deformation were modelled as elastic stringers with high Young modulus (figure 14). By doing so, one prevents building a computationally heavy model with convergence difficulties. This is done at the expense of obtaining higher deformation forces than those that are required in reality, since a component which is supposed to slide against the wing skin with negligible friction force is modelled as a stringer that needs to be stretched.

Aerodynamic loads are applied directly to the skin nodes as forces in the Cartesian reference frame. Since the aerodynamic mesh is different from the mesh used for the structural analysis (which is more refined), then forces in a particular location are evenly distributed around the surrounding skin nodes.

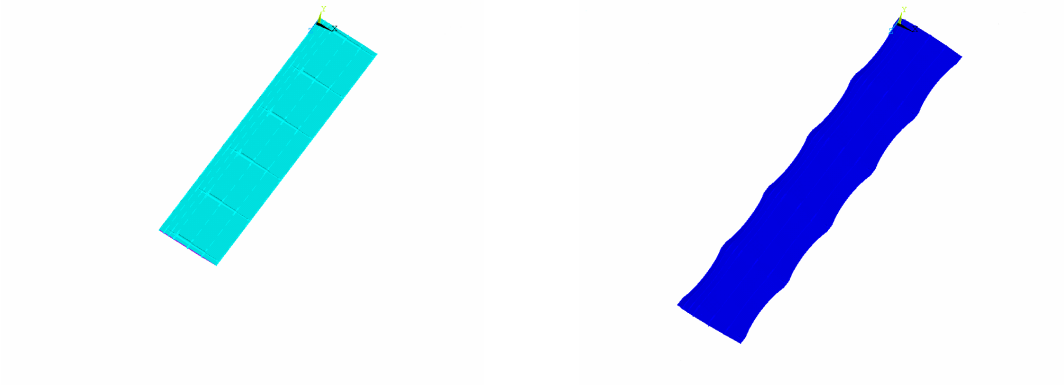

Figure 14 - *wing model showing (above) the undeformed and stretched skin*

A simple convergence study using a section of the wing was performed to assess the suitability of the FEM mesh. This study revealed that the refinement of the mesh could solve convergence problems but deformation forces and moments results did not differ significantly from a less refined mesh to a more refined mesh. Therefore, to reduce computation time requirements the least refined mesh was chosen to be used in the structural analysis and more refined meshes were used whenever convergence problems occurred.

In order to resist and transmit aerodynamic forces to the structure, the wing skin acting as a membrane must be stretched prior to the loading. However, the rubber material model used in this work becomes unstable at high stretches, say higher than 170%, which means that for a fully deformed wing a high initial stretch would cause model convergence problems. Therefore the initial stretch was adjusted to allow the full analysis of the wing for each flight condition, bearing in mind that, real rubber materials can stretch up to 300% and more and that this action will cause error in the prediction of deformation forces.

2.3 - Coupled Aero-Structural Analysis

The process used to estimate the morphing wing drag and structural requirements is illustrated in figure 15. At a given flight condition and aircraft weight, the aerodynamic optimization tool optimizes the wing shape and passes it together with the aerodynamic loads to the structural model. Here the structural control points are made coincident to the aerodynamic control points and the aerodynamic loads are distributed to the skin FEM nodes. Then, the structural analysis is carried out with the control points fixed and the deformations of the skin are obtained. In the next iteration, the new wing shape is

passed to the aerodynamic solver and new loads are computed. The process is repeated until convergence is achieved.

The convergence criterion for this coupled problem is based on the aerodynamic loads, because only these loads vary and cause different deformations on the structure. Once the aerodynamic loading is nearly constant after consecutive iterations, the deformed wing has its stationary shape for the current flight condition. Therefore, convergence is assumed when the force variation on each node falls below 1%.

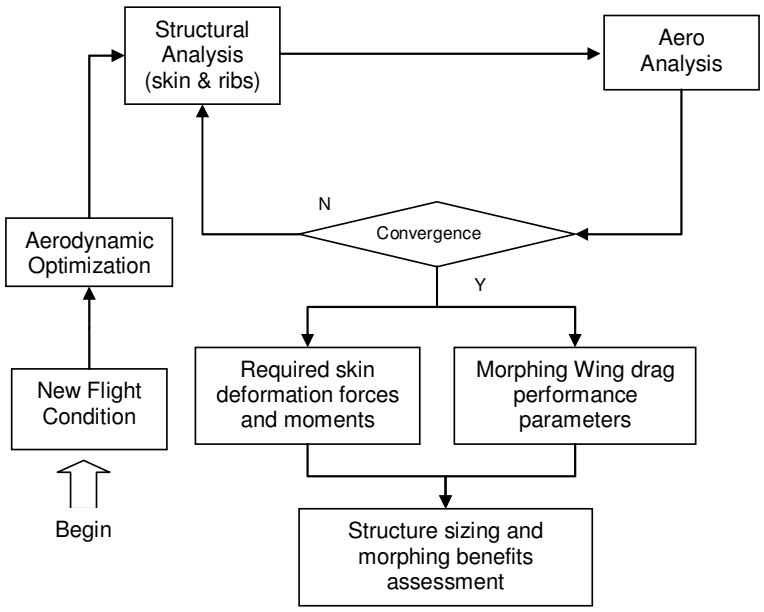

Figure 15 - *Flow chart of coupled aero-structural analysis of an optimum morphing wing at different flight speeds*

2.3.1 - Coupled Aero-structural Analysis Results

Since rubber is not a rigid material, when it is wrapped as a sleeve around the wing internal mechanism and structure with some level of pre-extension it tends to the shape shown in figure 16. Straight lines form between consecutive control points at any section and the chord and thickness reduce between consecutive ribs. As a result, the wing aerodynamic characteristics are different from the perfectly smooth optimized wing. The solution from the aero-structural analysis is shown in figure 16.

The deformation of the chord of the wing resulted in reduced wing area as can be seen by comparing figure 13 with figure 16. Wing drag was mainly affected by the section deformation. Induced drag remained almost unchanged.

Initially, a somewhat low pre-extension value was used in the skin model. Since the control points do not move for a given configuration, the surface of the airfoil exhibited undesired bumps between the control points due to the suction that exists around the airfoil. In figure 16, the airfoil for 40m/s clearly illustrates this effect. For the other speed cases, a higher pre-extension value of the rubber has already been used which enabled a more fixed shape with almost straight lines between control points. The pressure coefficient distributions around the wing illustrate the peaks of alternating zones of low pressure and high pressure that occur due to the small curvature of the wing surface at the control points.

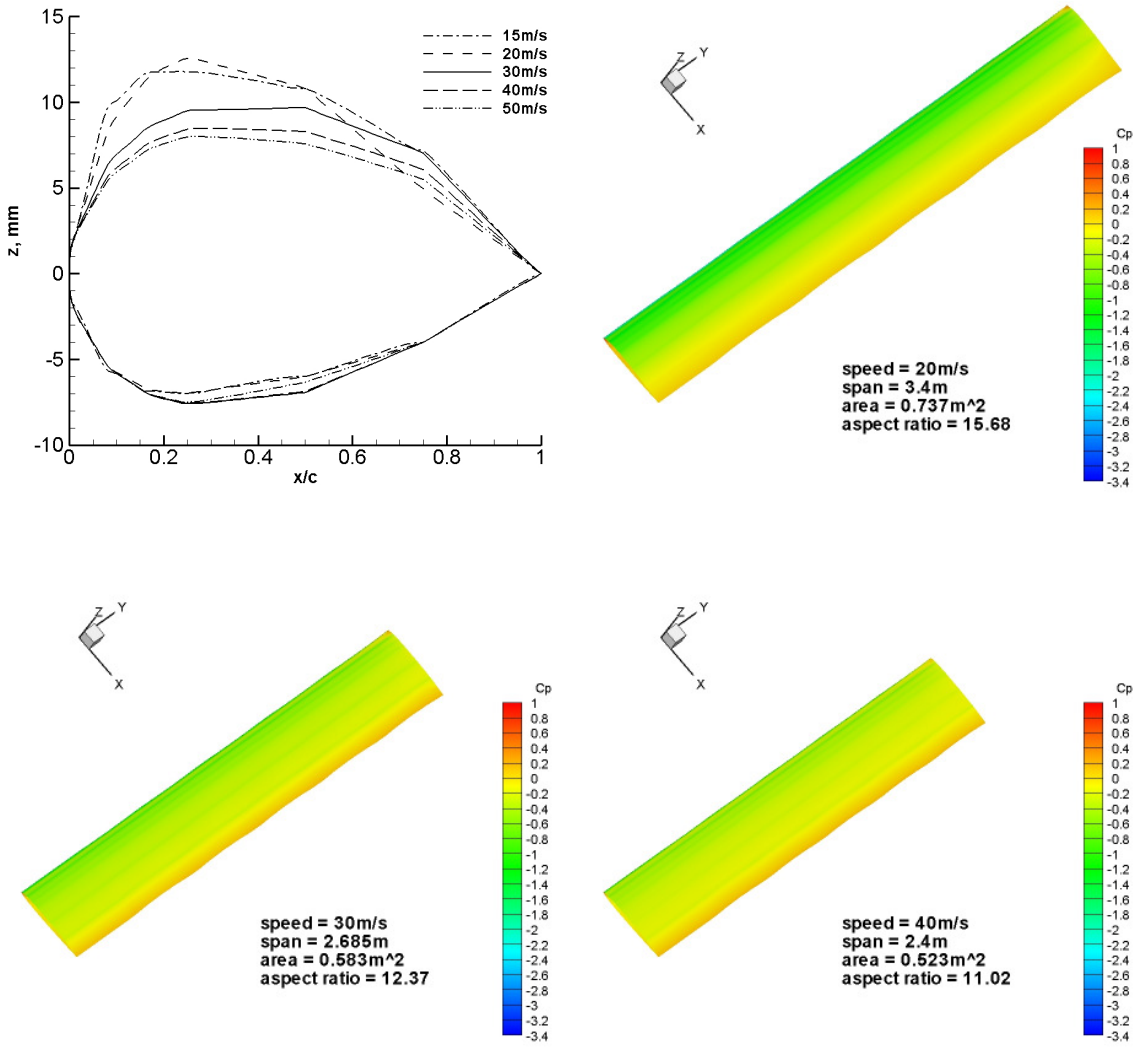

Figure 16 - *Airfoil sections at wing tip and wing planforms for five speeds from the aero-structural analysis*

2.4 - Wing Drag Results

When comparing the optimized morphing wing with the original wing drastic drag reductions are obtained at all speeds. Figure 17 illustrates well this. At the original wing cruise speed of 30m/s, drag has reduced by more than 50%. The morphing wing design, despite its shortcomings at low speeds due to the limited thickness changes that can be produced.

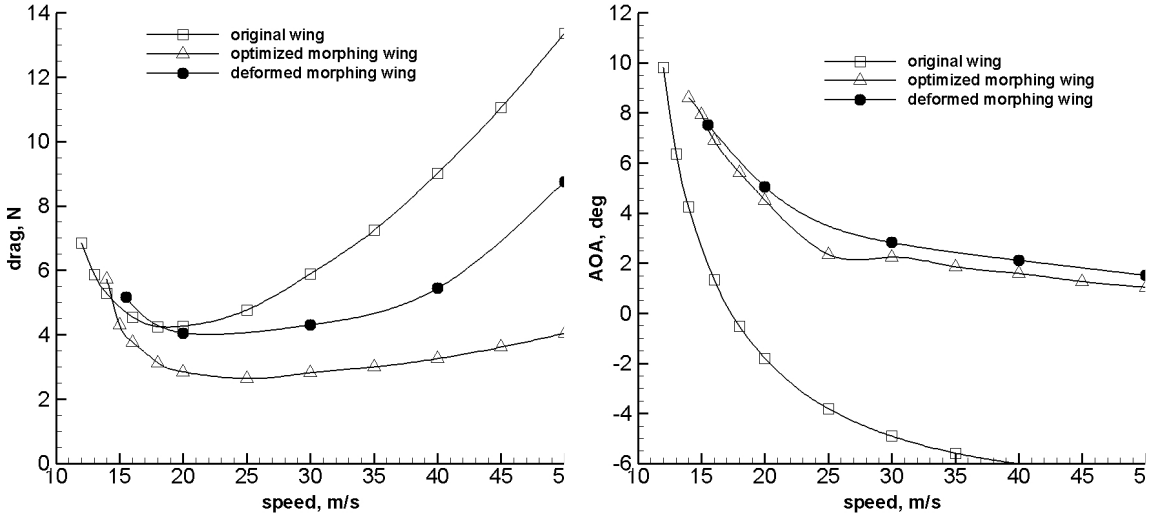

Figure 17 - *Comparison of drag and angle of attack estimates of the original wing, the optimized morphing wing and the deformed morphing wing for various flight speeds*

As anticipated, the performance of the deformed morphing wing is not so good. The skin surface deformation greatly influenced the parasite drag of this wing. The drag improvements are about half of those of the optimized morphing wing. For instance, at 30m/s the reduction in drag is 26.9%. There is a quite important shortcoming at low speed. Table 1 summarizes the percent reductions in drag obtained by the morphing wing.

WING	15M/S	20M/S	30M/S	40M/S	50M/S
optimized morphing	11.2	33.3	52.2	63.9	69.7
deformed morphing	-6.3	5.0	26.9	39.6	34.5

Table 1 - *Percent drag reductions with optimized morphing wing and deformed morphing wing*

One important advantage of the morphing wing is that the angle of attack between 25m/s and 50m/s varies only by 1.3deg. This situation helps in maintaining the fuselage

in an almost horizontal position for most of the speed range in straight and level flight, which for some surveillance applications may be of interest. On the other hand, fuselage drag can be reduced since it may be at a small angle of attack to the airflow.

2.4.1 - Morphing Wing Concept Limitations

The limitations imposed by the morphing concept described in this work are concerned with the degree of approximation to the optimized wing shape that the morphing mechanism is able to comply. The main differences between the optimized shape and the deformed wing shape consist of:

- Straightening of the wing sections between the ribs and consequent loss of wing area;
- Inability of the mechanism to provide the ribs with a smooth airfoil shape with curved lines between control points;
- The fixed leading edge radius becomes small when, at low speeds, the maximum thickness and camber positions move forward and the first control point stands out creating a good place to trigger separation;
- Finally, the mechanism's limitation in airfoil camber line changes, necessary for low speed flight.

Chapter 3

3 - Structural Design | Wing

This chapter describes the design and construction process of the morphing wing prototype. The structural forces and moments that the morphing mechanism is required to withstand were based on the deformation forces and moments obtained from the structural FEM model, [24].

The aim was to conceptualize a mechanism that allows chord and span to change, trying to approximate all possible wing planforms between the smallest area wing and the maximum area wing. Tapered and elliptical approximations are also possible to perform.

Minimizing weight is, definitely, very important in aerospace engineering but the main goal in this work is to assess whether the morphing concept works. Figure 18 shows the scheme of possible configurations.

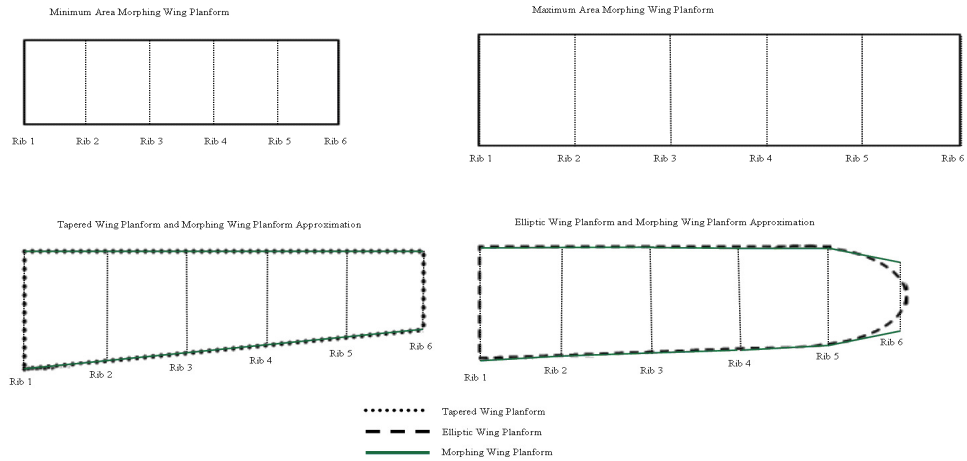

Figure 18 - *Morphing Mechanism conceptual capability*

The increase in span and chord length were assumed to be 50% of their smallest value. This condition is safely below the rupture strain of vulcanized rubber under equal biaxial loading, as described in [16].

Each chord expansion mechanism is independently actuated and allows different planform shapes to be obtained. At each rib section, independent servo-actuators are used to extend the chord in the leading edge and in the trailing edge directions, so that the quarter chord line can stay perpendicular to the wing root section.

3.1 - Morphing Mechanism Design for Wind Tunnel Testing

The structural FEM model produced the following results in terms of forces for a morphing wing with the capabilities described in the previous chapter in its fully extended position: the compressive force span wise is 8000N, compressive force chord wise is 1500N and compressive force along thickness 250N.

These total forces refer to the full scale half wing, which in its retracted state is 1m long span wise, 0.22m long chord wise and has a 0.002m thick rubber skin. In order to be possible to fit the model in the wind tunnel testing facility the model has to be reduced to half size. Therefore, span is 0.5m and chord is 0,11m. In order to reduce the actuation forces needed to deform the wing skin, the skin thickness was reduced to 1mm.

The wind tunnel model is assumed to increase span and chord in the proportions used for the full scale FEM model, which are 50% increase in span and chord dimensions. Therefore, the stresses levels on the skin must be caused by the mechanism and are the same of the full scale model.

For the normal stress in spanwise direction we have:

$$\sigma_{Fullscale} = \frac{F_{Fullscale}}{A_{Fullscale}} = \frac{F_{Fullscale}}{st_{Fullscale} sb_{Fullscale}} = \sigma_{Halfscale}$$

$$\frac{F_{Fullscale}}{st_{Fullscale} sc_{Fullscale}} = \frac{F_{Halfscale}}{\frac{st_{Fullscale}}{2}\frac{sc_{Fullscale}}{2}} \Rightarrow F_{Halfscale} = \frac{F_{Fullscale}}{4}$$

Where $\sigma_{Fullscale}$ is the stress on the full scale component model, $F_{Fullscale}$ is the force actuating on the component, $A_{Fullscale}$ in the area where the force is actuating, $st_{Fullsale}$ is the dimension chordwise of the component and $sc_{Fullscale}$ is the dimension along its thickness. The subscripts "*Half scale"* correspond to the half scale model.

This means that the actuation forces in the half scale model with half skin thickness are four times smaller relative to the full size model. The same reasoning can be used for the stress in the chord wise direction. For the forces in the wing thickness direction, the reasoning is slightly different since it depends on the wing sections' relative thickness. Assuming the final relative thickness of the half scale wing is approximately the same as the full scale one, the compressive force in the thickness direction is reduced to half, due to the reduction to half of the skin thickness.

Consequently, the sizing of the half scale wing model for wind tunnel testing is based on the following actuation forces: span wise force is 2000N, chord wise force is 375N and along the thickness the force is 125N.

Since the half scale wing dimensions are very small, the thickness of the wing sections doesn't allow the design of an economically and technically feasible airfoil morphing mechanism. Because of this, changing the wing airfoil thickness was discarded and only chord and span changes were considered for the morphing mechanism design. Naturally, changes in chord dimension changes the airfoil shape, but the airfoil thickness cannot be actively altered for a given chord length.

As can be seen in figure 19, the airfoil at each rib will have three fixed shape sections which will change their relative position along the chord axis as the total chord changes. All the other requirements and assumptions made for the full scale FEM modelling are taken into account in this new mechanism design.

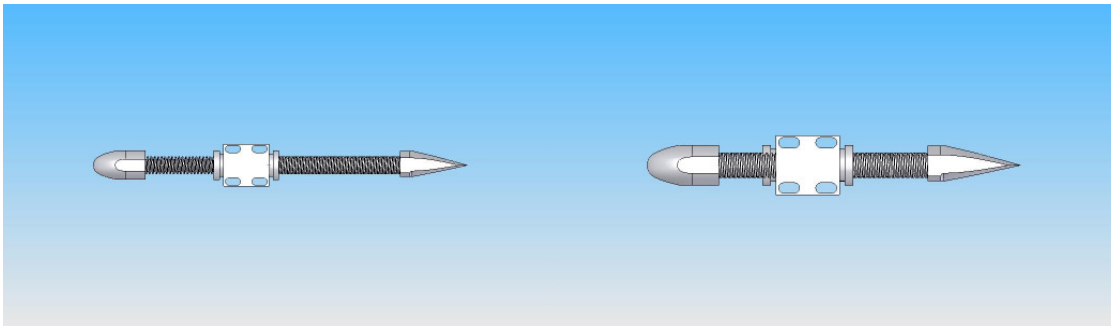

Figure 19 - *Designed rib extension mechanism: on the left extended, on the right retracted*

3.1.1 - Mechanism Design

In this design, a fixed block in each rib supports the whole rib structure and connects the whole mechanism with the spars while screws make translation motion through the

block core and stretch the wing skin. The block also supports the nuts which are mated to the screws and are the only moving parts of the rib, since they are rotationally actuated to cause the screws translation motion.

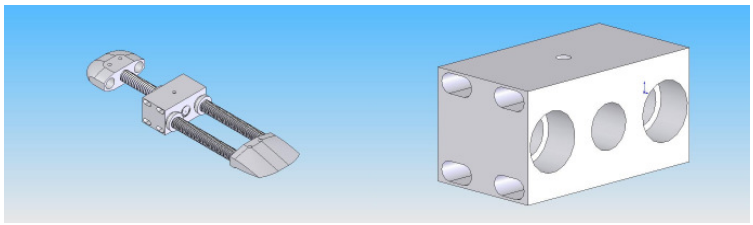

Figure 20 - *Rib parts: on the left assembled rib expansion mechanism; on the right central block*

Attached to the tip of the screws are the leading edge and trailing edge blocks. These blocks have the function of shaping the wing skin at the leading and trailing edge, respectively, and also serve as support elements for the leading and trailing edge shaping beams, as can be seen in figure 20.

As it happens with the leading and trailing edge blocks, the function of these extendable beams is to maintain the leading and trailing edge shape in the wing sections between ribs. The beams are connected to the leading and trailing edge block through hinges to allow taper in the wing sections between ribs, shown in figure 21.

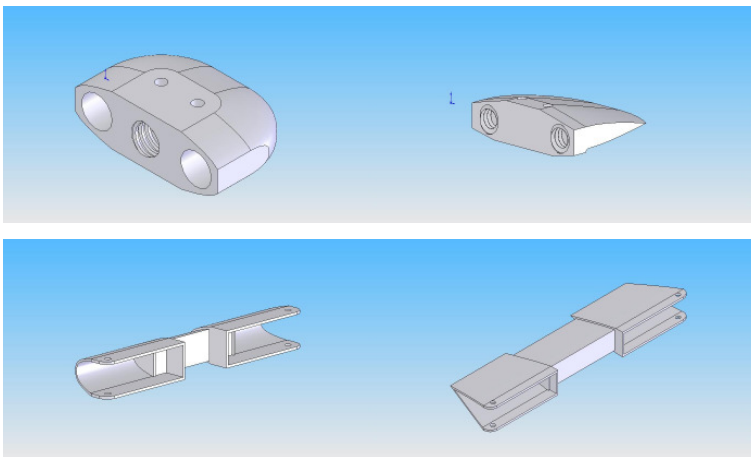

Figure 21 - *Rib parts: on top left leading edge block; on top right trailing edge block ;on bottom left leading edge shaping beams; on bottom right trailing edge shaping beams*

With this design, each rib is actuated independently through the use of chains that rotate the screw nuts. This will allow greater freedom in obtaining the optimized wing planform shape, although it will increase wing weight (figure 22). This is possible by

using twelve electric motors attached to the ribs, two per rib, and transmitting the motion with chains to the rotating nuts.

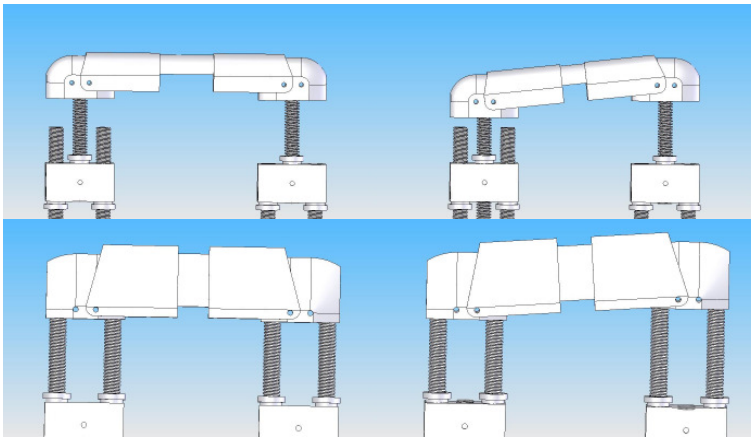

Figure 22 - *Leading and trailing edge beams assembly with the rib expansion mechanisms: top left: straight leading edge assembly; top right: tapered leading edge assembly; bottom left: straight trailing edge assembly; bottom right tapered trailing edge assembly*

The span extension mechanism is based on beams that are pulled through the use of actuation which can be manual or motorized, rotating nuts that pull the actuation plate (the cross shaped plate) and make it slide along the threaded beams on figure 23, stretching the wing skin. The number of beams and their position is a function of the loading and geometric constraints of the wing sections. This mechanism also includes the hinged structure that places the ribs equally spaced along the span, as in the first design.

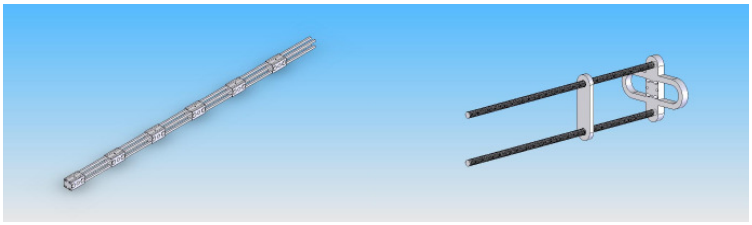

Figure 23 - *Span extension mechanism: on the right: spar expansion mechanism and on the left span actuation mechanism*

In order to extend the wing span, the wing spars must be pushed in the spanwise direction. Thus, an actuation mechanism was designed based in screws, nuts and rubber bands. This mechanism ensures a uniform space between ribs by using the rubber bands to connect them. If all rubber bands have the same elastic constant, the same displacement will cause the same reaction force for all rubber bands that keep the spacing.

The mechanism assembly can be seen in figure 19. The actuation plate pushes the spars and is supported by the threaded shafts that are fixed to the wing root cross-shaped plate. The horizontal extensions of the root plate are used for clamping the wing skin. The complete mechanism assembly is shown in figure 24.

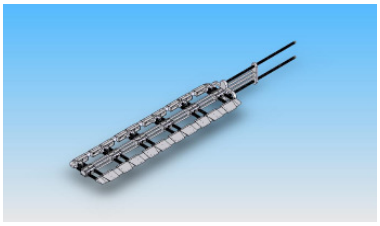

Figure 24 - *Complete assembly of the morphing wing structure*

3.1.2 - Mechanism Sizing

Spatial considerations are of paramount importance due to the high forces involved and the small space available to fit the morphing mechanism that will support all the loads.

The first mechanism parts to be sized are the critical elements that support direct loadings and produce the motion of the mechanism. Those parts include the rib threaded shafts, the spars and the spars actuation mechanism threaded shafts. Other important parts are the tip, root and actuation plates, since they will be subject to the same loads as the previous parts. Although in this case no buckling is of concern. These parts were analyzed and sized based on the FEM results alone to make sure that the allowed stress was not exceeded. The rotating rib nuts and the actuation mechanism nuts were sized analytically. This comprised the definition of the necessary threaded length of the nuts to support the loadings and also the necessary nut thickness. FEM analysis were then used to confirm stress levels on the nuts unthreaded thickness. Also the gearing of the nuts were done analytically. The remaining parts (central block, leading edge and trailing edge blocks and beams) were sized based on the wing geometry. Due to their higher dimensions FEM analysis were made only to confirm stress levels. Finally, the pins that are used to connect some of the mechanism parts (leading and trailing edge blocks connect with the leading and trailing beams) were sized to withstand pure shear in the connection surface.

In order to simplify the analysis, the threads of the various threaded parts were not included in any of the FEM analysis mentioned above. Figure 20 shows the FEM

meshes and loads of the designed parts together with the stress results from the FEM analysis.

3.1.3 - Sizing of Rib Threaded Shafts

The sizing of the rib shafts was based on the maximum actuation force per rib times a safety factor of 1.25 which gives the design load of 469N, a compression force acting on the clamped shaft. Aluminium was chosen as the material for the rib shafts with the characteristics shown in table 2 [14].

Material	*E, GPa*	*v*	σ_{yield} *Tension, MPa*	σ_{yield} *Compression, MPa*	$\tau_{ultimate}$, *MPa*
Aluminium	72	0.33	345	345	283
Steel	200	0.3	345	345	-
Acrylic	2.2	0.3	47	100	-

Table 2 - *Material mechanical properties*

The critical shaft would be the leading edge shaft because it supports all the compressive loading alone while the two trailing edge shafts support half the load each. Nevertheless the maximum length of the trailing edge shafts is higher and this is relevant for the buckling load calculation. Therefore, the shaft analyses took into account the maximum loading times the safety factor and the maximum shaft length, assuring structure stability in a conservative manner.

Analytical, linear FEM and nonlinear FEM analyses were performed to calculate the buckling loads and stresses on the rib threaded shafts (figure 25). The analytical calculation is based on the following expression for the buckling load of a perfect column with a clamping support:

$$P_{cr} = \frac{EI\pi^2}{(2l)^2} \quad (1)$$

Where P_{cr} is the buckling loading, E is the Young Modulus, I is the second area moment and l is the length

This expression is used in others analytical critical load calculations. Results are shown in table 3.

Part	*Material*	*Load, N*	*Diam. x Lengh, mm*	*P_{cr} Euler, N*	*P_{cr} Linear FEM, N*	*σ_{VM}, MPa*
Rib Shaft	Aluminium	-489	7x96.25	-2260.13	-2258.98	93.6
Spars (eccentric load)	Steel	-2000	4x750	-3953.32	-3133.80	335
Spars (skin & spars non-linear FEM)	Steel	-1794	4x750	-	-	307
Spars actuation shaft	Aluminium	1250	6x330	-	-	44.2

Table 3 - *Rib threaded shaft, spars actuation shafts sizing results*

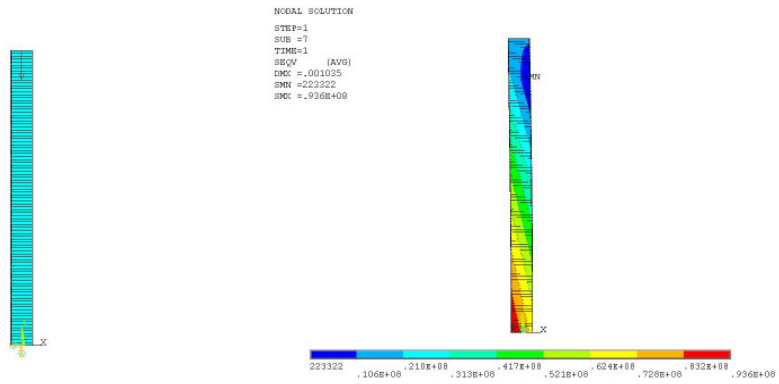

Figure 25 *- on the left: rib threaded shaft FEM mesh; rib threaded shaft equivalent Von Mises stress*

3.1.3.1 – Sizing of the Spars

The spars were sized based on the span wise actuation force multiplied by a safety factor of 1.25 which gives a design load of 2500N, a compression force acting on a clamped beam. The calculations showed that for the spar the material should be steel. The properties of steel are shown in table 3.

A compromise between the available space and the necessary second moment of area to support the loading had to be made. Also, the compression load is eccentric relative to the spars centroid when it reaches its maximum, since the spars geometrical centre is positioned at ¼ of the chord length from the leading edge. To work as spars, 8 small steel beams with 4mm diameter were distributed inside the central block area. FEM analysis shows that the constraints on the beams' displacement, imposed by the rib blocks, increase the critical load and prevent excessive displacements.

Analytically we made a linear FEM and nonlinear FEM analyses to calculate the buckling loads, stress and deformation due to the eccentric loading. Analytical calculations of the buckling load in the two principal directions were done without consideration for the eccentricity of the load. A FEM nonlinear analysis was performed using two models: one displaces the load from the centroid of the spars by a calculated amount and another includes the skin material and forces it to stretch in a similar way as the wing skin. This last analysis has shown the necessary skin deformation forces to be considerably lower than the design loading assumed (figure 26). Results are shown in table 2. For all this analysis it was used beam elements for the beams and shell elements for the skin. The mesh was automatically generated due to the simple geometry of these parts.

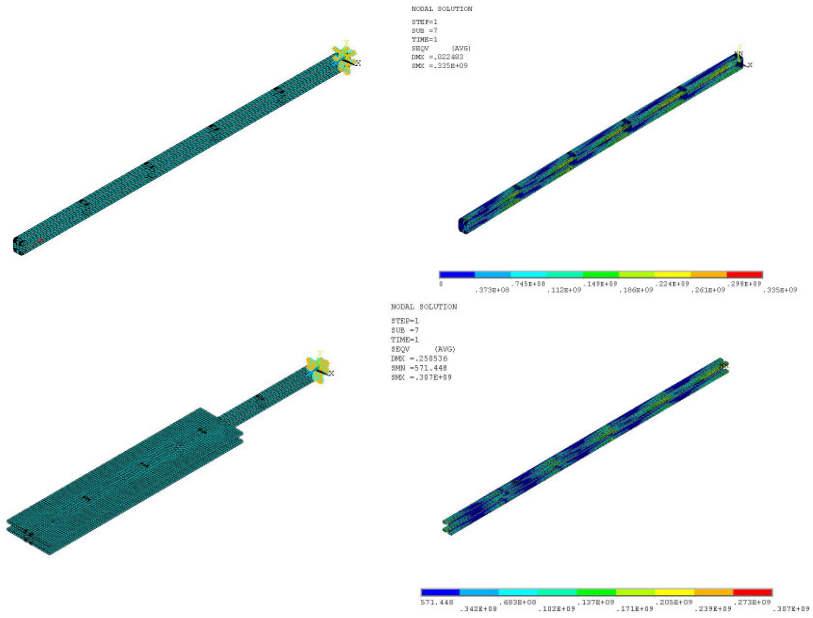

Figure 26 *– on the top left: spar eccentrically loaded FEM mesh; on the top right: spar eccentrically loaded equivalent Von Mises stress; on the bottom left: spar and skin FEM mesh; on the bottom right: spar equivalent Von Mises stress*

3.1.3.2 – Spars Actuation Mechanism Threaded Shafts

Since the shafts are subject to tension, not compression as the previous ones, a simple stress calculation was made to determine the shaft inner diameter. Results are shown in table 3.

3.1.3.3 – Tip, Root and Actuation Plates

The sizing of these plates consists of defining only the thickness of the plates in order to keep the stress level under an acceptable value. Results are shown in table 4.

Part	*Material*	*Total Load, N*	*Thickness, mm*	σ_{VM} *,Mpa*
Tip Plate	Aluminium	2500	4	194
Root Plate	Aluminium	2500	10	317
Actuation Plate	Aluminium	2500	5	270

Table 4 - *Tip, root and actuation plates sizing results*

3.1.3.4 - Rotating Rib Nut

The rotating rib nut has to be thick enough to withstand the compressive loading of the rib threaded shaft and also long enough so that the threaded length is sufficient to support the shear stress caused by the loaded shaft.

The calculation of the threaded length (L_e) is based on the approximate formula shown below [17],

$$\tau_{\max} = \frac{F}{A_s}, \quad (2)$$

where $\tau_{\max}$ is the allowed shear stress for the nut material and A_s is the shear resistive area of the nut. A_s is given by:

$$A_s = \frac{\pi}{2} d_p L_e, \ (3)$$

where d_p is the pitch circle diameter of the thread, which is given approximately by:

$$d_p = D - 0.64952\,p, \ \ (4)$$

Thus, the minimum threaded length of the nut/screw is given by (5):

$$L_e = \frac{2F}{\pi(D - 0.64952p)\tau_{\max}}, \quad (5)$$

Although these formulas are approximate, they give conservative results. As a result, FEM analysis was used to obtain the stress levels on the nut, assuring that the nut was correctly dimensioned. Results are shown in table 5.

Part	*Material*	*Total Load, N*	*Thickness, mm*	*D, mm*	*p, mm*	*L_e, mm*	*A_s,,mm^2*	*τ, MPa*	*σ_{VM}, MPa*
Rotating rib nut	Aluminium	489	1	9.24	2	9	113	4.15	33.6
Actuation nut	Aluminium	1250	3	15	5	10	145	8.61	14.9

Table 5 - *Rotating rib and actuation nuts' sizing results*

3.1.3.5 - Actuation Mechanism Nuts

The sizing process of these nuts is based on the same assumption made for the rotating rib nut, but with different loading, since these nuts support the spanwise loading of the structure. FEM analysis was used to obtain the stress levels of the nut. Results are shown in table 4.

3.1.3.6 - Central Block, Leading and Trailing Edge Blocks and Beams

Due to the complexity of the geometry of these parts they were imported to *Ansys*© from the *SolidWorks*©. Since the actuating forces were low, the mesh was created automatically; the areas where the mesh had numerical problems were fixed manually. These parts were the only ones to use solid elements. The analysis using FEM showed that all stress level were acceptable, as it was expected. Due to this result the material chosen was acrylic, since it is easier to machinate and hard enough to waistband the tests (figure 27).

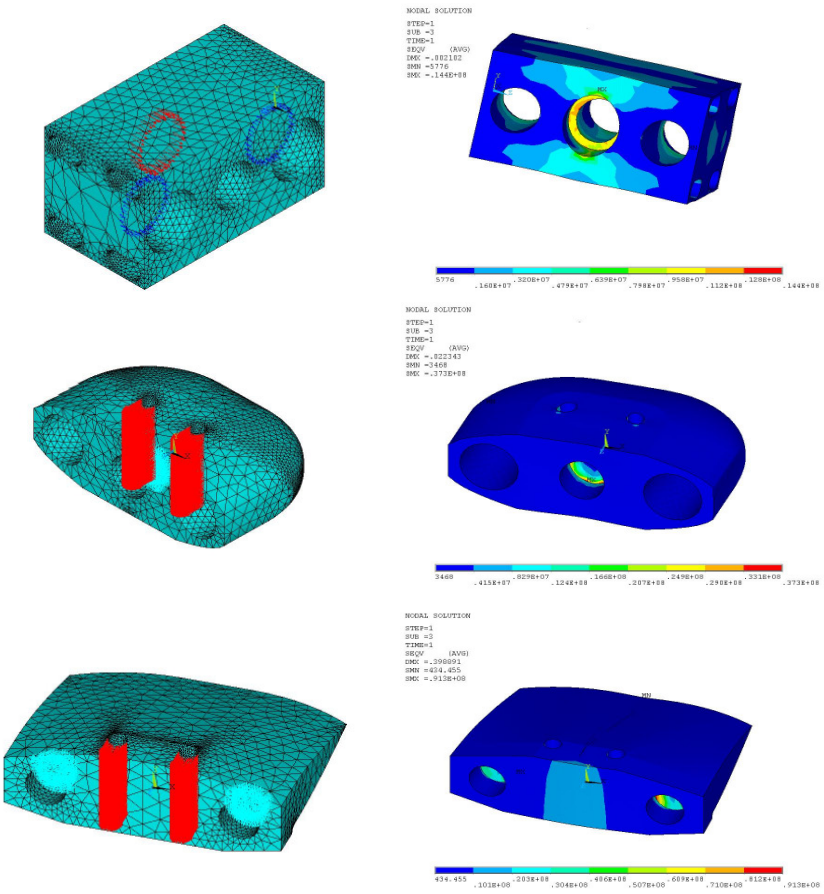

Figure 27 *- on the top left: central block FEM mesh; on the top right: central block equivalent Von Mises stress; on the middle left: leading edge block FEM mesh; on the middle right: leading edge block equivalent Von Mises stress; on the bottom left: trailing edge block FEM mesh; on the bottom right: trailing edge block equivalent Von Mises stress*

3.1.3.7 - Connecting Pins

These pins connect the leading and trailing edge blocks to the beams. The surfaces of these components are together. For that reason, these pins are sized to withstand pure shear. Results are shown in table 6.

Part	*Material*	*Total Load, N*	*Diameter, mm*	*τ, MPa*
Pin	Aluminium	489	3	69.2

Table 6 - *Rotating rib and actuation nuts sizing results*

3.1.3.7 - Actuation Torque Requirements

For the calculation of the actuation torque needed for rib and actuation nuts we calculate the torque needed to raise a load supported by a fastened screw. This calculation is based on the following expressions [20]:

$$M = F\frac{d_p}{2}\left[\frac{\left(\cos\left(\frac{\theta_n}{2}\right)\tan(\beta)+f\right)}{\cos\left(\frac{\theta_n}{2}\right)-f\,\tan(\beta)}\right]+FR_m f^{'}; \qquad (6)$$

$$\frac{\theta_n}{2} = a\tan\left[\tan\left(\frac{\theta}{2}\right)\cos(\beta)\right]; \quad (7)$$

$$\beta = a\tan\left(\frac{p}{\pi d_p}\right); \qquad (8)$$

The first term of the equation 6 represents the necessary torque to overcome the friction between the threads of the screw and nut while the second term represents the necessary torque to overcome the friction between the nut and the support surface where the nut lies on. Equation 7 relates the angle between the reaction force and the axis of the screw with the screw parameters θ and β, where θ is the thread profile angle and β is given by equation 8. Results for the maximum torque are shown in table 7.

Part	*Material*	*Total Load, N*	*p, mm*	*d_p, mm*	*θ, º*	*f*	*f'*	*M, Nm*
Rotating rib nut	Aluminium	489	2	7.99	29	0.3	0.3	1.49
Actuation nut	Aluminium	1250	5	9.24	29	0.3	0.3	5.47

Table 7 - *Rotating rib and actuation nuts torque requirements*

3.2 - Wing Manufacturing

Construction of the designed mechanism took place at I.S.T mechanical laboratory for mechanical tooling. The main tool used was the milling machine. This machine has six degrees of freedom, three rotations and three translation degrees and a digital position indicator, which allows precision until centesimo of millimetre. This tool has revealed to be very powerful, since its six degrees of freedom allowed to machine all the parts of the wing structure and make the final assembly. The milling machine had recesses in the gears, so the precision of the work was less than expected.

The available tooling machines allowed a limited precision in making holes and keeping the alignment of the relatively great number of pieces to be manufactured. As a consequence, the spar extension mechanism used to equalize the distance between ribs as the span increases revealed to be extremely ineffective. Other affected parts that due to alignment difficulties couldn't withstand the loading were the expanding beams from both the leading and trailing edge. The torsional stiffness of the eight spars was also very low, because the tolerances involved were not able to constrain the eight spars to act as a single spar. Finally, the friction force between the rotating rib nuts and the central block was very high, both in the initial requirements and in the actual mechanism assembly.

The screws and the rotating nuts were made by an exterior technician. We made the order specifying the screws' pitch and exterior diameter. For the nuts we specified exterior dimensions to fit these nuts in the central blocks (figure 28).

Figure 28 - *Shaft and rotating nut*

All other parts were made by us, using the milling machine. The leading and trailing edge beams were made with a folding machine. All the other parts of the wing were made in the milling machine (figure 29).

Figure 29 - *Leading and trailing edge sliding beams*

The interior parts of the leading and trailing edge were made at the milling machine as well as the leading and trailing edge blocks. The inclined surfaces were made by using one of the rotations of the milling machine (figure 30).

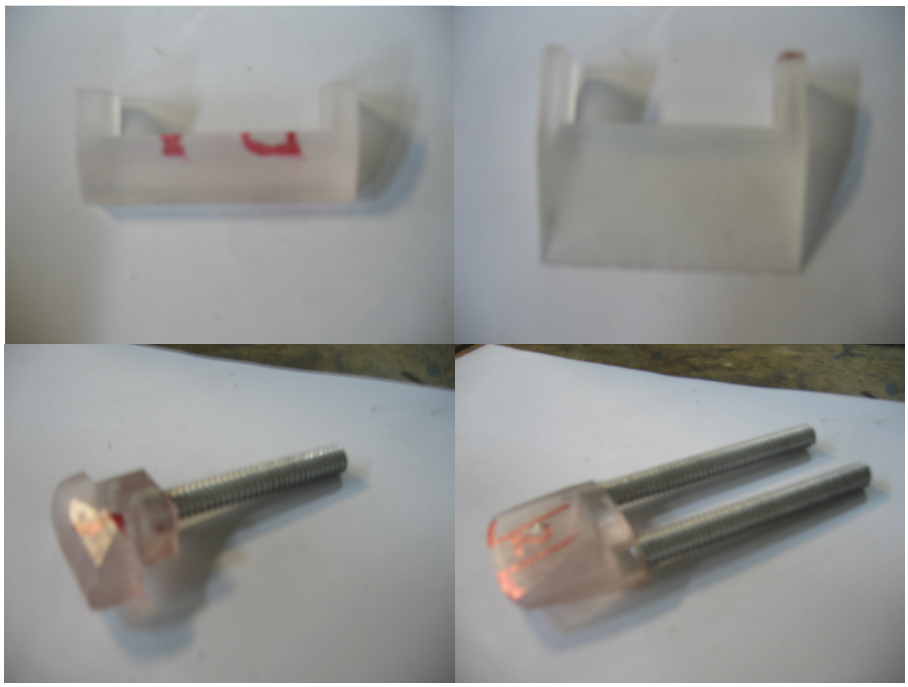

Figure 30 - *Leading and trailing edges made in acrylic*

The central blocks were made using a cylinder of 25mm of diameter. The milling machine was used to create the rectangular shape of the crossing section of 22x24mm. Then the holes were drilled. The chord wise holes were easy to make. The holes in span direction were not so easy to drill, because these holes are deep and the driller has to be

longer. Once it is hard to have a perfectly balanced drill, the drill's tip vibrations make it impossible to keep the holes aligned (figure 31).

Figure 31 - *Central block*

The resulting rib is the one in the next photo.

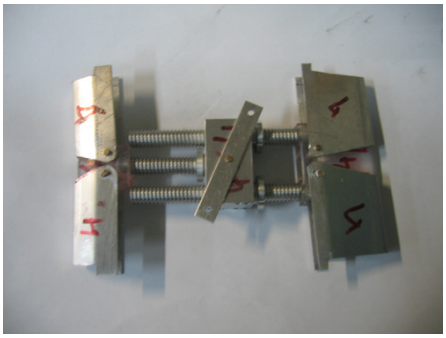

Figure 32 - *Assemble rib*

The wing accomplished the entire requirements pre-established and allowed the chord and the span to vary. The next photos are the wing fully extended in the left side and the fully retracted in the right side (figure 33).

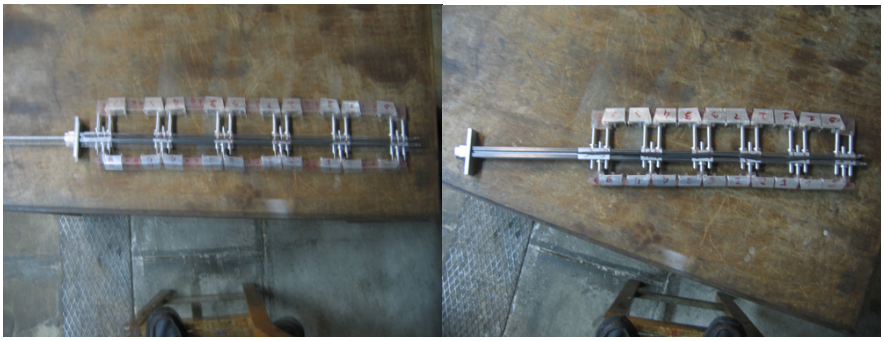

Figure 33 - *Assemble wing: in the left: extended; on the right: retracted*

All of the problems described above were solved with several improvements made during the construction of the final prototype and also by changing the wing skin material for a less stiff material.

The span extension mechanism equalizer was substituted by rubber bands connecting the neighbouring ribs. This solution, although dependable on the stiffness of the rubber bands used and the friction between the central blocks and the spars, worked quite well for the precision required and resulted in wing weight loss.

Dropping the requirement of making the mechanism able to produce different wing planform shapes than rectangular and tapered shapes allowed the expanding leading and trailing edge beams to be substituted by solid sliding beams with the leading and trailing edges shapes, respectively.

The eight spars were substituted by a long U shaped plate which greatly increased the torsional stiffness, because it could be made in a whole piece by bending the plate in the desired shape. Since the thickness of the plate was the same thickness of the spars, no loss of bending stiffness occurred with this change. The spar was now over dimensioned for the rubber stretching force requirements and with this change there was a weight increasing. However, this part can later be substituted by a molded carbon fibre composite which will reduce greatly the weight penalty.

In order to reduce the actuation force requirements, two different measures were taken: the friction surface of the rotating rib nuts was reduced by diminishing their length L_e, avoiding contact of the lower surface of the rib with the central block and at the same time reducing the contact area around the nut; skin material was changed for a less stiff one, reducing the complete set of forces involved in the initial design. The natural rubber initially chosen for the skin was substituted by a new composite material with rubber like behaviour made of licra fibre in a matrix of silicone rubber. This material is described in the next subsection.

In conclusion, some of the parts described previously were found to be useless; such were the tip plate, the excessively over dimensioned cruciform root plate and the double shaft mechanism for the span extension. Figure 34 shows the final mechanism assembly, which can be compared to the one of figure 33.

Figure 34 - *Final mechanism assembly*

Because of these changes in the mechanism design, the final dimensions of the prototype in the chord dimension had to be slightly changed, in the smallest chords, from 0.11m to 0.12m. However, there is still an increase in the chord and span, in 50% of their smallest dimensions. Table 8 summarizes the final prototype dimensions and its span and chord range, as well as the relative thickness variations, possible maximum thickness relative chord position variations and taper ratio range.

Dimension	*b/2, m*	*c, m*	*t/c*	*λ*	*A*	*Max t/c Pos, %*	*D_{LE} ,mm*
Variation Range	0.5-0.75	0.12-0.18	0.122-0.183	0.667-1	5.56-12.50	25-56	16.0

Table 8 - *Final morphing mechanism dimensions ranges*

3.2.1 - New Skin Material Description

The new skin material was conceived having in mind some requirements. In order to allow the study of the morphing wing benefits and also understand the behaviour of a wing covered with a flexible material: it should allow high levels of strain and the manufacturing process should be such that the stiffness of the material could be changed, either through the increase of material thickness, constitution or both.

Given the resources available, we chose, after some preliminary experiments, to use licra fibre, which allows high strains of over 150%, inserted into a matrix of silicone that allows very high strains and is impermeable to air. The number of fibre layers and the amount of silicone used serve to control the stiffness of the material which is manufactured.

The manufacturing process was manual and so the properties of the materials fabricated would change from piece to piece. Also surfaces from very rough to very smooth were

obtained depending on the manufacturing process (figure 35). All of these conditions contribute to the difficulty of characterizing the material used. Nevertheless some studies on the behaviour of such a skin were made.

Figure 35 - *Licra fibre in silicone matrix composite material for the wing skin*

Chapter 4

4 - Wind Tunnel Test

Wind tunnel testing took place at AFA aeronautical laboratory facility. A blow-down wind tunnel with closed circuit was used. The balance to measure aerodynamic forces and moments was fixed at the centre of the working section. Thus an adaptation had to be made in order to install the half span wing prototype. Since this work is focused on drag and lift and their relation on the morphing wing, there was no need to calculate the transfer of moments through the supporting structure that was assembled to place the wing root aligned with the wind tunnel wall.

4.1 - Tests

The supporting structure consisted of a bended beam clamped at the scale to act as an arm and place the wing root to the side of the wind tunnel test section (figure 36).

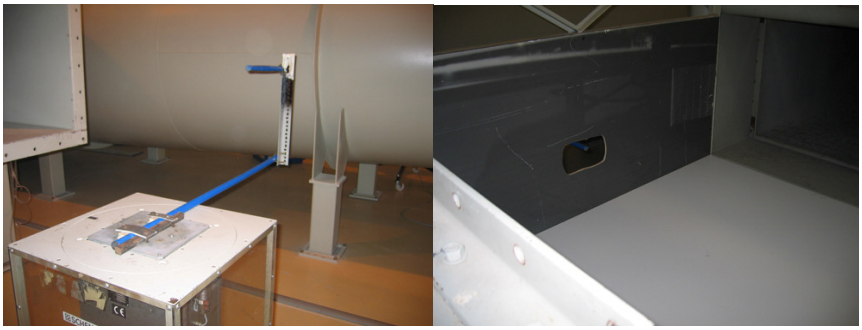

Figure 36 - *Wind tunnel testing assembly: on the left: Supporting structure connected to the scale on the right: Bottom and side plate placed at the wind tunnel section*

To avoid interference of this structure with the airflow and therefore prevent measuring structure drag along with wing drag, a table was used over it. For the same reason, a plate with a hole was placed aligned with the wind tunnel section side. The morphing wing was connected to the supporting structure outside the wind tunnel section and inserted into the test section through the hole in the side plate. Figure 17 shows the testing assembly.

The use of the bottom and side plates incurred in some lift corrections because of ground effect and mirror effect [6]. The side plate causes the lift to increase to double as it works as a mirror for the airflow and the bottom plate causes an increase in lift depending on the proximity of the wing to the plate.

Table 9 shows the lift increase as a function of the span to distance to the ground ratio obtained from ref. [6]. Linear interpolation was used to calculate the corrections for the tested planform shapes of the morphing wing.

h/b	*L/ L_{Ref}*
5	1.01
1	1.02
0.5	1.05
0.2	1.14

Table 9 - *Lift corrections for ground effect*

The lift corrections are needed in order to assess the amount of lift that the wing is expected to produce, to allow a direct comparison between morphing wing configurations and the original UAV wing.

Dimensional analysis between areas is used to calculate the lift which the prototype wing is supposed to produce. From this point, the lift produced by the morphing wing with any planform configuration should be the same. The lift corrections are then calculated for each planform configuration to assess the points that should be searched for in terms of lift and drag for drag performance comparison at different wing configurations. Table 10 shows the area and expected lift for the prototype wing.

Wing	*b, m*	*c, m*	*Area, m^2*	*A*	*L, N*
Original	2.4	0.33	0.792	7.273	100.00
Original without Fuselage	2.0	0.33	0.660	6.061	83.33
Prototype	1.0	0.18	0.180	5.556	22.73

Table 10 - *Lift relations between original and scaled wing*

Note that the prototype wing is not geometrically scaled to the original wing, since the aspect ratio is not maintained. As it was said before, the actual span of the morphing wing without considering the fuselage would be 2m, which is the length that

corresponds to the 1m span of the prototype. The final mechanism's dimensions with the necessary changes slightly changed the wing scaling, because of the minimum and maximum chord values. Nevertheless, since the aspect ratio of the prototype is less than the one of the original wing and the prototype area is slightly higher than expected for a perfectly scaled prototype, the drag performance should be worse and so the drag results are conservative when the benefits are concerned.

4.1.1 - Tested Configurations of the Morphing Wing

Five planform shapes of the morphing wing have been tested. The first four configurations' sequence is consistent with the optimization results obtained previously [24], as can be seen in table 11, where the four configurations' planform dimensions and lift corrections are given. These results show the wing tending to its maximum area configuration at low speeds, changing to tapered form at maximum span, lowest chord and maximum span and finally lowest chord and lowest span as speed increases.

Configuration	*b, m*	c_{Tip}, *m*	C_{Root}, *m*	*Area,* m^2	*h/b*	L/L_{Ref}	*L, N*
1	1.5	0.18	0.18	0.270	0.227	1.132	25.73
2	1.5	0.12	0.18	0.225	0.227	1.132	25.73
3	1.5	0.12	0.12	0.180	0.227	1.132	25.73
4	1	0.12	0.12	0.120	0.34	1.098	24.95
5	1	0.18	0.18	0.180	0.34	1.098	24.95

Table 11 - *Tested configurations' geometries and expected lift*

During the test, it was found that the inability to actively change the airfoil thickness was crucial, since the relative thickness increases as the chord is decreased. Thus, at high speed, when chord is retracted, relative thickness is very high, whereas at these high speeds the relative thickness should be small. Consequently, a fifth configuration was considered: maximum chord and minimum span.

Wind tunnel tests were also performed to determine the influence of the initial stretch of the wing skin and its rigidity in the wing aerodynamics. The different skins were tested at configuration 4. This configuration has the smallest wing planform and therefore the skin isn't so stretched. Consequently, if the skin has not instability problems for the

entire speed range, these problems will not come up if we use a bigger wing. Since the objective was to evaluate the different skins, none of the measurements taken were corrected due to the influence of the walls near the model, because all of then had the same influence.

Chapter 5

5 - Results Analysis

In this chapter results obtained on the wind tunnel tests are described and also analysed. First the different skins results are presented to validate which has the best behaviour at different speeds. Then the different configurations results are presented

5.1 - Detail Analysis

During the tests, several observations were made: the flexible skin deforms due to the pressure field of the flow; the deformation becomes higher at higher airspeeds and as the speed increases the pressure decreases carrying to higher deformations; over certain airspeed the vibration of the skin produced noise and cyclic deformations.

These observations leaded us to the study of the influence of the skin stretch and skin stiffness, on the aerodynamics of the flexible skin wing. Therefore, using the morphing wing at configuration four, experiments were made with the wing stretched at two different expansions and also with a skin made of a double number of lycra fibre layers and with a double overall thickness. Table 12 presents the skins characteristics.

Skin	*Spanwise stretch*	*Chordwise stretch*	*Nº of licra fibre layers*	*Thickness, mm*
1	1.05	1.325	2	1
2	1.29	1.25	2	1
3	1.05	1.325	4	2

Table 12 - *Tested skins characteristics*

The results shown on the graphics of the figures 37 and 38 correspond to the configuration 4 with three different skins. The charts are lift coefficient (C_L) versus angle of attack (AoA) and Drag (D) versus Lift (L), for the different airspeeds (U) for which the tests were performed.

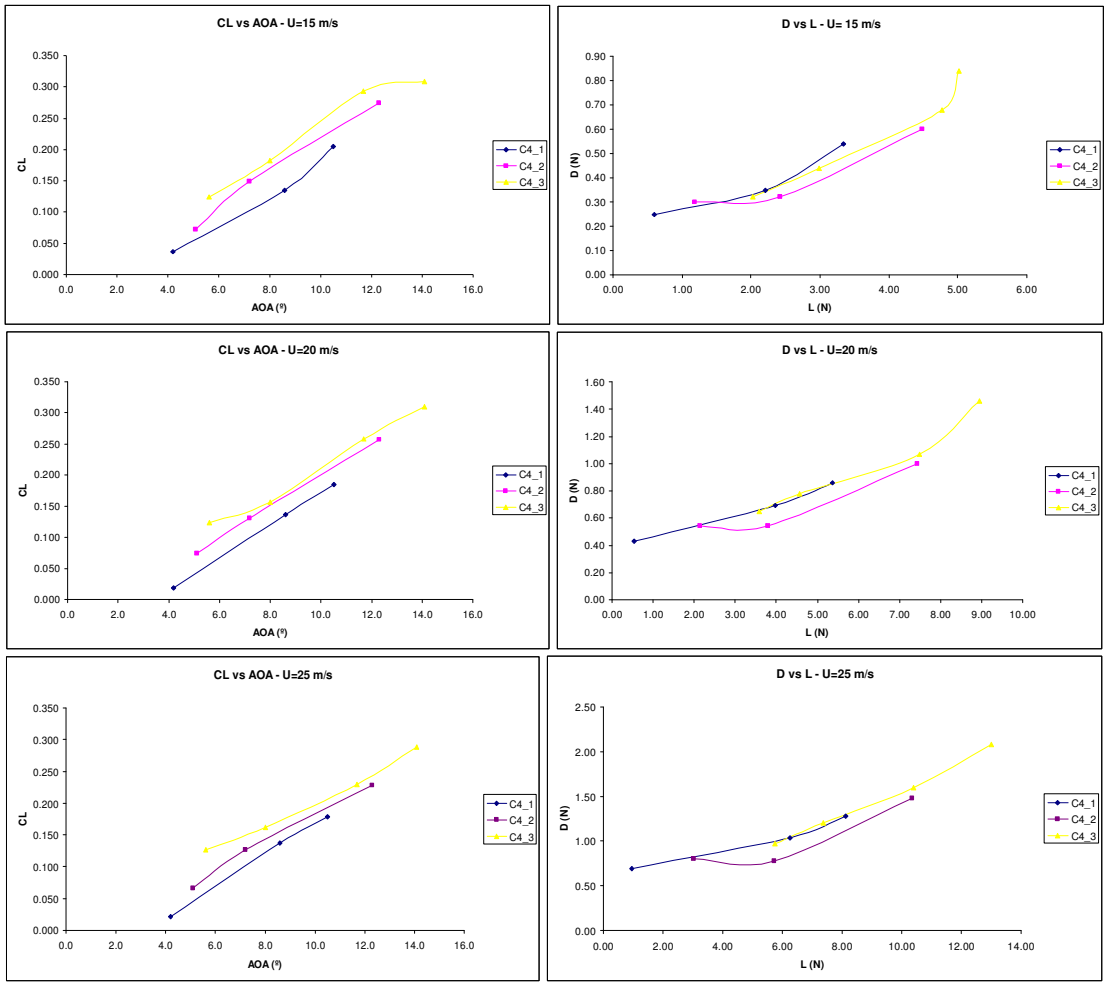

Figure 37 - *Aerodynamic forces results for the three different skins tested for configuration 4 at 15, 20 and 25 m/s airspeed*

As it can be seen on the charts above (figure 37), for the first three airspeeds (15, 20 and 25 m/s) the effect of increasing the stiffness or the stretch of the skin is an increase in CL; however, a reduction in drag is observed only when the stretch is increased (data set C4_2). This observation is explained by lower deformations of the stretched skin, preventing the wing sections from becoming thicker and therefore reducing pressure drag.

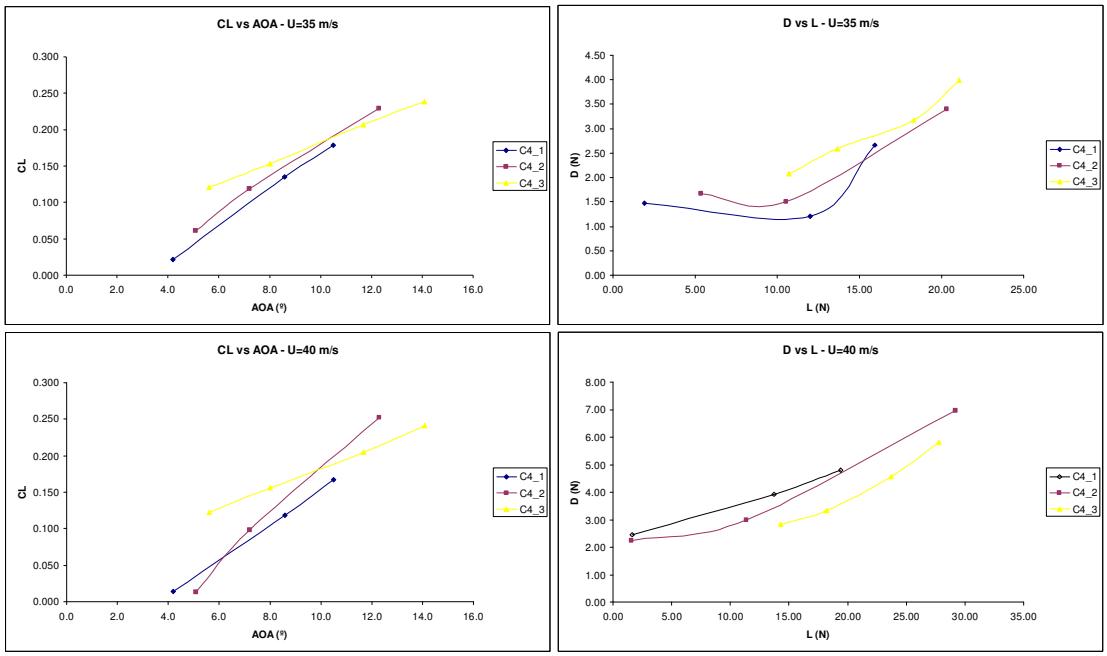

Figure 38 - *Aerodynamic forces results for the tested skins at 35 and 40 m/s airspeed*

When looking at the D versus L curves at the referred velocities, it is observed that for the same stretch (data sets C4_1 and C4_3) the values of drag are similar for the same lift values. The increase in the thickness of the airfoil due to the thicker skin may explain the higher CL observed at the same AOA when comparing with the thinner skin. The advantage of having a stiffer skin is to have the same lift at a lower AOA.

Between airspeeds of 35 and 40 m/s (figure 38) the occurrence of skin instability was observed for skins 1 and 2, which did not happen with skin 3. This occurrence is visible in the difference of slope of the CL versus AOA curves (CL_α). For the thicker skin CL_α is lower, although D versus L curve shows that the skin instability happens sooner in thinner skins.

In figure 39 is shown the influence of airspeed in CL_α and the drag coefficient (CD) for skin 3. It can be verified that as speed increases, CL_α decreases while the CD varies without showing a clear tendency. This is caused by the deformation of the skin, which alters the wing sections and reduces the wing's efficiency. Similar trends were verified for skins 1 and 2.

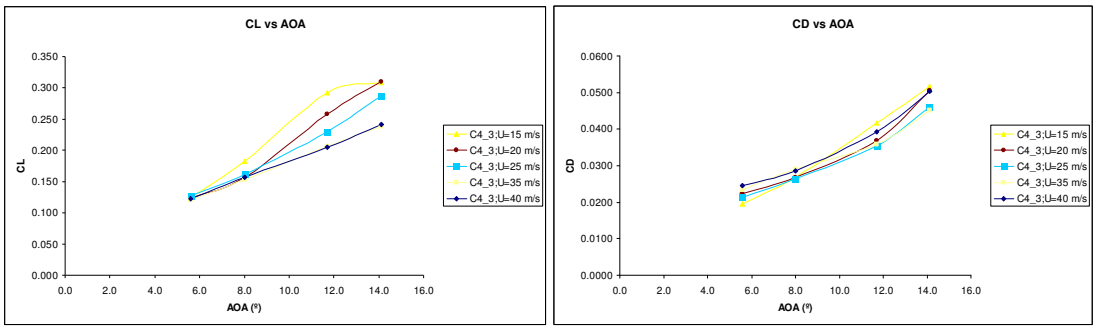

Figure 39 - *Influence of airspeed in CLα and CD for skin 3*

The testing of different wing configurations was done using skin 3. This skin was the one that maintained a reasonable performance at higher speeds, allowing a wider range of airspeeds for comparisons between wing configurations.

5.1.1 - Morphing Wing Configurations Comparison

The tested configurations produced the following results depicted in figures 40 and 41.

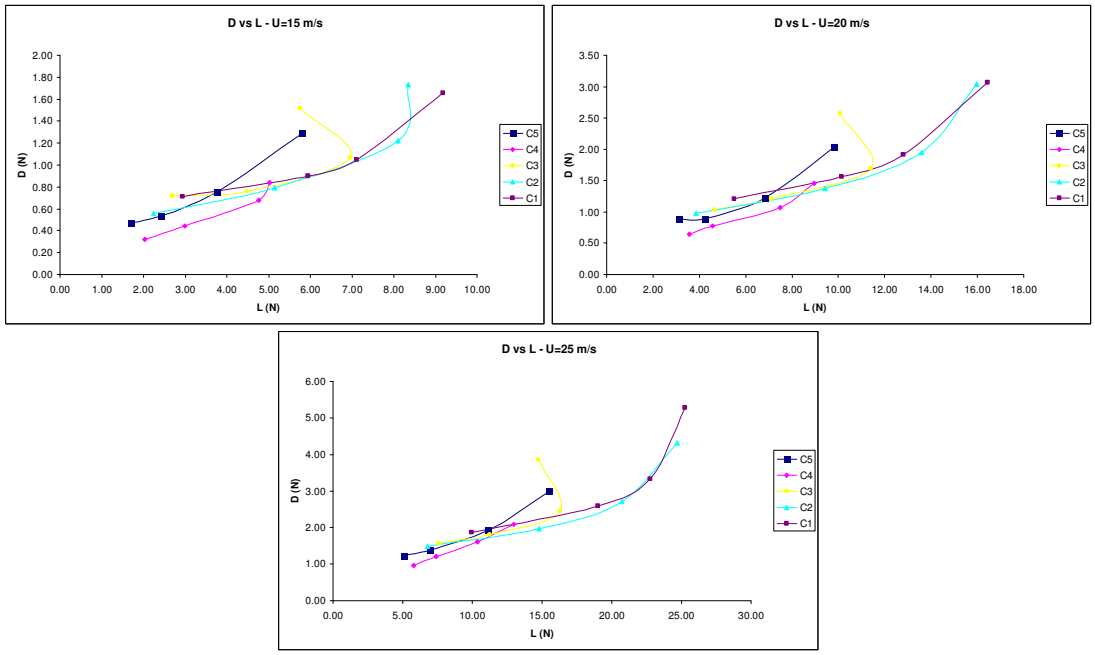

Figure 40 - *Drag versus lift curves for 15, 20 and 25 m/s airspeeds and wing planform configurations*

From the graphics above (figure 40), configurations 3, 4 and 5 do not produce the necessary lift, of about 25N, at speeds below 35m/s and configuration 1 and 2 do not produce the necessary lift at speeds below 25m/s.

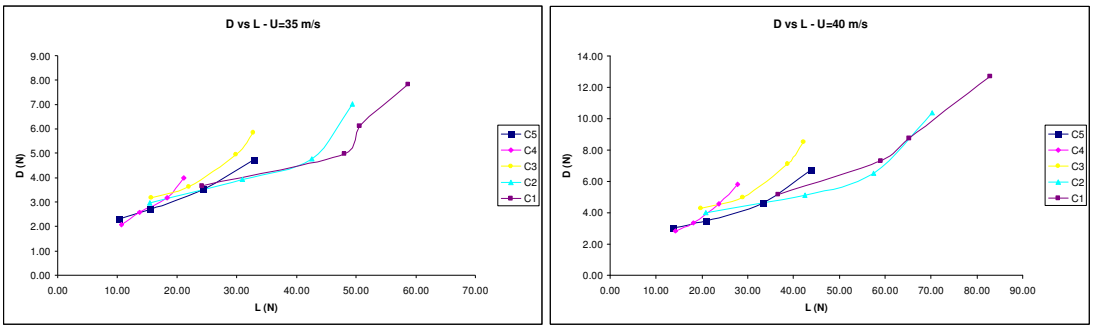

Figure 41 - *Drag versus lift curves for 35 and 40 m/s airspeeds and wing planform configurations*

Consequently, the stall speed of the morphing wing for the fully loaded UAV would be around 25m/s. The reason for this huge increase in stall speed, when compared to the stall speed obtained in the computational study (15 m/s) lies in: the poor aerodynamics of the morphing wing airfoils, which are symmetrical, the high thickness of the airfoil and the fact that the maximum thickness position, that is close to middle chord station when the wing chord is fully extended.

The reduction of the necessary lift that the wing is supposed to produce obviously decreases the stall speed. Depending on the required lift, the configurations that are most advantageous at different speeds may vary. Tables 13 to 15 show the drag values obtained from the drag versus lift curves by interpolation, for different values of lift.

Configuration	Lift (N)	Drag (N)		
		U=40m/s	U=35m/s	U=25m/s
1	25.73	4.92	3.74	5.74
2	25.73	4.18	3.57	**4.56**
3	25.73	4.51	4.11	
4	24.95	4.90	5.00	
5	24.95	**3.65**	**3.37**	

Table 13 - *Morphing wing drag for different planform configurations at different airspeeds for a 22.73 N required lift*

From the results shown above we can see that choosing to start the flight with the wing at configuration 2 at 25m/s, we can obtain a drag reduction of 12.6% at 40m/s, if we morph the wing to configuration 5 (table 15).

Configuration	Lift (N)	Drag (N)		
		U=40m/s	U=35m/s	U=25m/s
1	20.376	5.04	3.44	2.54
2	20.376	4.02	3.25	**2.43**
3	20.376	4.29	3.41	
4	19.764	3.62	3.60	
5	19.764	**3.28**	**2.86**	

Table 14 - *Morphing wing drag for different planform at different airspeeds for a 18.00 N required lift*

The same result can be obtained if the required lift is about 18N: the drag reductions at 40m/s can achieve 18.3%, as the wing is morphed again from configuration 2 to configuration 5.

Configuration	Lift (N)	Drag (N)		
		U=40m/s	U=35m/s	U=25m/s
1	15.282	5.29	3.16	2.21
2	15.282	3.93	2.96	**1.91**
3	15.282	4.57	3.18	2.28
4	14.823	**2.89**	**2.64**	2.43
5	14.823	3.10	2.49	2.77

Table 15 - *Morphing wing drag for different planform configurations at different airspeeds for a 13.50 N required lift*

For a required lift of 13.5N the wing should start the flight at configuration 1 or 2 for speed of 20m/s, morphing to configuration 2 at 25m/s, then morphing to configuration 5 at 35 m/s and finally to configuration 4 at 40m/s. At the end of the morphing process the

drag reduction would be 26.3%, when the wing is at configuration 4 instead of configuration 2.

Note that on configurations 3 and 4, drag performance is not the one expected. When comparing the planform shapes of these configurations with configuration 5, their drag performance should be superior, since the areas are less or equal and the aspect ratio is higher than the ones of configuration 5. The reason why this is not so, is due to the increasing of wing's relative thickness when the chord is retracted, as well as the lower stretch level that the wing skin is submitted to in these configurations, that causes the skin to deform and alter the wing sections geometry more easily.

These results show that although the morphing wing with the flexible skin does not allow active control of the wing sections shapes, some significant drag reductions can be obtained. Reducing the thickness of the wing while the chord is retracted will benefit the high speed configurations. On the other hand increasing the airfoils curvature at lower speeds is also beneficial.

Chapter 6

6 - Synthesis

6.1 - Conclusions

A computational study was performed, revealing that significant improvements in drag performance of a wing can be obtained by changing the wing's span, chord and airfoil [23]. These studies served as motivation to design, build and test a morphing wing with flexible skin in which the span and chord can be changed.

During the manufacturing process some conclusions were taken. Some components revealed to be non-functional. The spacing mechanism initially designed did not work. The reason for this was the tolerances involved; we found that the tolerances had to be very small. The connecting pins had to be tight enough for the space bars not to move freely, but at the same time the recess had to be enough to let the same bars move when needed. We had not enough precision to make this mechanism. As a result we replaced it for rubber bands connecting the ribs.

The rubber bands connecting the ribs were able to keep the same spacing between the ribs. Since these bands were the same, each time one is stretched the whole system reacts to the stable position, characterized by equal stretching in all bands.

The leading and trailing edge blocks and beams initially thought to be in aluminium were made of acrylic. We made this change after the evaluation of the endurance of the aluminium. The whole structure initially was projected to be made of aluminium; however, having all components in the same material would cause fatigue. Another reason to change the material was the easiness to machine acrylic.

The spars didn't behave like we expected, the torsional stiffness was very low. Therefore, the eight beams were replaced by a "*U*" shaped beam to increase the torsional stiffness. Also the leading and trailing edge beams were replaced by a single beam with the shape of the leading and trailing edge. This two measures increase greatly the torsional stiffness of the wing.

The wing's structure resulting was able to fulfil the requirements previously set.

Influence of stretch and stiffness of the wing's skin on the aerodynamics of the wing was studied. Increasing the wing's stretch helps approximate the wing to a rigid skin wing, therefore approximating the aerodynamics of the wing to what is usually seen in aerodynamics studies. The increase in skin stiffness helps to prevent the occurrence of skin instability at high speeds. However, higher skin's stiffness drives to a higher actuation force and higher loads upon the structure. As a result, the structure should be stronger, which increases the weight.

The results obtained on the wind tests of the morphing wing show that drag reductions up to 45% could be obtained with this wing, when we compare the take off wing with the high speed wing.

Configuration five confirmed that the relative thickness for configuration four was very high, leading to poor results. Configuration three also did not achieve the results expected for the same reason. The wing tip cross section has a very high relative thickness.

The results have showed that we were able to use a morphing mechanism to reduce drag, while maintaining the lift required. The reduction of drag is due to the reduction of wing area, since at higher speeds we can use smaller wings to produce the same lift.

6.2 - Further Work

Further work should be focus on improvement of the weakness revealed by our mechanism. A mechanism able to change actively the thickness and to make the airfoil thinner for higher speeds would be a very important development.
Another weakness of the solution presented is the difficulty of scaling up the model. Therefore, an alternative skin solution should be searched.
In figure 42 a possible solution to change actively the thickness is shown.

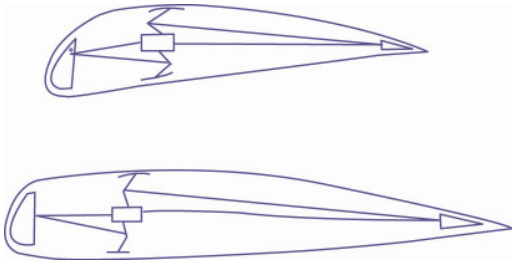

Figure 42 - Solution to change actively the thickness

With this kind of solution when the chord is extended or retracted the thickness also increases or decreases. As a result, the relative thickness may be kept constant.

The solution presented will require a high actuation force due to the skin. The bigger wing surface leads to a more stretched skin, increasing the tension on it. To overtake this problem a screen cover with a flat plate solution can be very helpful, since the force required to actuate this mechanism is not dependent on the wing surface, as it is sketched in figure 43.

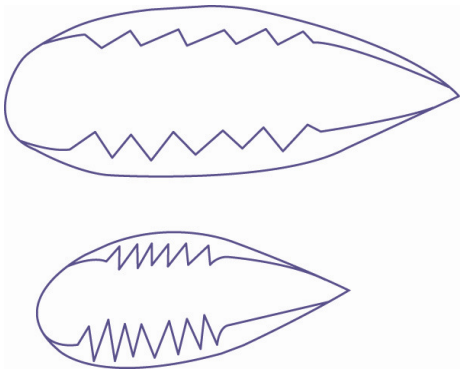

Figure 43 - Solution to decrease to actuation force

The flat plate will give the wing airfoil shape and prevent the turbulence that will be created by the screen.

References

[1] M. Abdulrahim, “Flight Dynamics and Control of an Aircraft with Segmented Control Surfaces”, University of Florida, AIAA-RSC2-2003-U-010.

[2] M. Abdulrahim and J. Cocquyt, “Development of mission capable flexible wing micro air vehicles”, University of Florida, Gainesville, FL 32611-6250, 2002.

[3] Anderson, J. D., Corda, S., and Wie, D. M. V., “Numerical Lifting Line Theory Applied to Drooped Leading-Edge Wings Below and Above Stall,” *Journal of Aircraft*, Vol. 17, No. 12, 1980, pp. 898-904.

[4] Jae-Sung Bae, T. M. Seigler, D. J. Inman, Virginia Polytechnic Institute and State University, Blacksburg, VA 24061, USAand In Lee Korea Advanced Institute of Science and Technology, Daejon 305-701, Korea, “Aerodynamic and Aeroelastic Considerations of A Variable-Span Morphing Wing”

[5] P. Bourdin, A. Gatto and M. I. Friswell, “The Application of Variable Cant Angle Winglets for Morphing Aircraft Control”, University of Bristol, AIAA2006-3660, 2006.

[6] V. Brederode, *“Fundamentos de Aerodinâmica Incompressível”*, Author’s ed., 1997

[7] D. Cadogan, T. Smith, F. Uhelsky and M. MacKusick, “Morphing Inflatable Wing Development for Compact Package Unmanned Aerial Vehicles”, AIAA2004-1807, 2004.

[8] P. Gamboa, P. Aleixo, J. Vale, F. Lau, A. Suleman, “Design and Testing of a Morphing Wing for an Experimental UAV”, RTO-MP-AVT-146

[9] L. Gonzalez, “Morphing Wing Using Shape Memory Alloy: A Concept Proposal”, University of Puerto Rico, 2005.

[10] M. T. Kikuta, “Mechanical Properties of Candidate Materials for Morphing Wings”, University of Virginia, December 2003.

[11] O. L. Majer, “The Application of Smart Actuators in the Development of a Model Plane Wing”, Union College, June 2006.

[12] J. E. Manzo, “Analysis and design of a hyper elliptical cambered span morphing aircraft wing”, Cornell University, 2006.

[13] www.matweb.com, March 2007

[14] D. A. Neal III, “Design, Development, and Analysis of a Morphing Aircraft Model for Wing Tunnel Experimentation”, University of Virginia, April 2006.

[15] S. O’Donnel, “Nanotechnology Trends in Materials and Their Impact on Aviation”, MITRE Corporation, 2004

[16] polymerfem.com/modules.php?name=Materials_Models&material=8, March 2007

[17] www.roymech.co.uk, March 2007

[18] B. Sanders U.S. Air Force Research Laboratory,Wright–Patterson Air Force Base, Ohio 45433 F. E. Eastep University of Dayton, Dayton, Ohio 45469 and E. Forster U.S. Air Force Research Laboratory,Wright–Patterson Air Force Base, Ohio 45433, “Aerodynamic and Aeroelastic Characteristics of Wings with Conformal Control Surfaces for Morphing Aircraft”

[19] T. M. Seigler, “Dynamics and Control of Morphing Aircraft”, University of Virginia, 2005.

[20] J. E. Shigley and C. R Mischke, “*Mechanical Engineering Design”*, 7th ed., McGraw Hill, 2003.

[21] A. Shuetze, “Carbon Nanotubes”, University of Victoria, 2006.

[22] M. D. Stubbs, “Kinematic Design and Analysis of a Morphing Wing”, Virginia Polytechnic Institute and State University, 2003.

[23] M. Usui, J. D. Jacob and S. W. Smith, University of Kentucky, and Stephen E. Scarborough and David P. Cadogan ILC Dover “Second Generation Inflatable/Rigidizable Wings for Low-Density Flight Applications“

[24] J. Vale, F. Lau, and A. Suleman, IDMEC-Instituto Superior Tecnico, Lisbon, Portugal; and P. Gamboa, Universidade da Beira Interior, Covilha, “Optimization of a Morphing Wing Based on Coupled Aerodynamic and Structural Constraints”, Portugal AIAA-2007-1890